Inflammatory and regenerative processes in bioresorbable synthetic pulmonary valves up to two years in sheep: Spatiotemporal insights augmented by Raman microspectroscopy

Acta Biomaterialia 135 (2021) 243–259

Contents lists available at ScienceDirect

Acta Biomaterialia

journal homepage: www.elsevier.com/locate/actbio

Full length article

Inflammatory and regenerative processes in bioresorbable synthetic pulmonary valves up to two years in sheep–Spatiotemporal insights augmented by Raman microspectroscopy

B.J. De Kort[a,b], J. Marzi[c,d,e], E.M. Brauchle[c,d,e], A.M. Lichauco[a,b], H.S. Bauer[f], A. Serrero[f], S. Dekker[a], M.A.J. Cox[f], F.J. Schoen[g], K. Schenke-Layland[c,d,e,h], C.V.C. Bouten[a,b], A.I.P.M. Smits[a,b,*]

[a] Department of Biomedical Engineering, Eindhoven University of Technology, Eindhoven, Netherlands
[b] Institute for Complex Molecular Systems (ICMS), Eindhoven University of Technology, Eindhoven, Netherlands
[c] NMI Natural and Medical Sciences Institute at the University of Tübingen, Reutlingen, Germany
[d] Cluster of Excellence iFIT (EXC 2180) "Image-Guided and Functionally Instructed Tumor Therapies", Eberhard Karls University Tübingen, Tübingen, Germany
[e] Department of Biomedical Engineering, Eberhard Karls University Tübingen, Tübingen, Germany
[f] Xeltis B.V., Eindhoven, Netherlands
[g] Department of Pathology, Brigham and Women's Hospital, Harvard Medical School, Boston, MA, USA
[h] Department of Medicine/Cardiology, Cardiovascular Research Laboratories, David Geffen School of Medicine at UCLA, Los Angeles, CA, USA

ARTICLE INFO

Article history:
Received 17 May 2021
Revised 18 August 2021
Accepted 6 September 2021
Available online 10 September 2021

Keywords:
Tissue-engineered heart valve (TEHV)
In situ tissue engineering
Endogenous tissue restoration
Biomaterial
Foreign body response
Guided tissue regeneration

ABSTRACT

In situ heart valve tissue engineering is an emerging approach in which resorbable, off-the-shelf available scaffolds are used to induce endogenous heart valve restoration. Such scaffolds are designed to recruit endogenous cells *in vivo*, which subsequently resorb polymer and produce and remodel new valvular tissue *in situ*. Recently, preclinical studies using electrospun supramolecular elastomeric valvular grafts have shown that this approach enables *in situ* regeneration of pulmonary valves with long-term functionality *in vivo*. However, the evolution and mechanisms of inflammation, polymer absorption and tissue regeneration are largely unknown, and adverse valve remodeling and intra- and inter-valvular variability have been reported. Therefore, the goal of the present study was to gain a mechanistic understanding of the *in vivo* regenerative processes by combining routine histology and immunohistochemistry, using a comprehensive sheep-specific antibody panel, with Raman microspectroscopy for the spatiotemporal analysis of *in situ* tissue-engineered pulmonary valves with follow-up to 24 months from a previous preclinical study in sheep. The analyses revealed a strong spatial heterogeneity in the influx of inflammatory cells, graft resorption, and foreign body giant cells. Collagen maturation occurred predominantly between 6 and 12 months after implantation, which was accompanied by a progressive switch to a more quiescent phenotype of infiltrating cells with properties of valvular interstitial cells. Variability among specimens in the extent of tissue remodeling was observed for follow-up times after 6 months. Taken together, these findings advance the understanding of key events and mechanisms in material-driven *in situ* heart valve tissue engineering.

Statement of significance

This study describes for the first time the long-term *in vivo* inflammatory and regenerative processes that underly *in situ* heart valve tissue engineering using resorbable synthetic scaffolds. Using a unique combinatorial analysis of immunohistochemistry and Raman microspectroscopy, important spatiotemporal variability in graft resorption and tissue formation was pinpointed in *in situ* tissue-engineered heart valves, with a follow-up time of up to 24 months in sheep. This variability was correlated to heterogenous regional cellular repopulation, most likely instigated by region-specific differences in surrounding tissue and hemodynamics. The findings of this research contribute to the mechanistic understanding of *in situ*

* Corresponding author at: Department of Biomedical Engineering, Eindhoven University of Technology, Eindhoven, Netherlands.
E-mail address: a.i.p.m.smits@tue.nl (A.I.P.M. Smits).

https://doi.org/10.1016/j.actbio.2021.09.005

tissue engineering using resorbable synthetics, which is necessary to enable rational design of improved grafts, and ensure safe and robust clinical translation.

1. Introduction

Surgical or interventional valve replacement is the standard of care treatment for most patients with severe symptomatic valvular heart disease, and this treatment improves quality of life and prolongs survival. Surgical valve replacement with either mechanical or tissue valve substitutes (the latter composed of animal or human tissue and thus often called bioprostheses) generally yield favorable long-term outcomes; survival is 50-70% at 10-15 years following valve replacement [1]. Nevertheless, valve-related problems necessitate reoperation or cause death in more than half of patients with substitute valves within 10-15 years postoperatively [2,3]. Mechanical valves induce platelet deposition and blood coagulation, (i.e., thrombosis) necessitating lifelong anticoagulation to reduce the risk of prosthetic valve-related blood clots in patients receiving them. In contrast, bioprostheses have low potential for thrombosis. However, despite improvements in tissue treatments intended to enhance durability, bioprostheses frequently suffer structural valve degeneration, often resulting from calcification, which is particularly accelerated in children and young adults [4].

Recently, the principle of *in situ* tissue engineering (TE), also known as endogenous tissue restoration (ETR), has emerged as a promising alternative [5–7]. This approach utilizes the regenerative capacity of the human body to transform a resorbable polymeric implant into a living functional valve, directly in its functional site, or *in situ*. The resorbable graft functions as a suitable valve immediately upon implantation, and subsequently serves as an instructive template for progressive endogenous cell infiltration and tissue deposition [5,8]. Preclinical studies demonstrate the potential of *in situ* heart valve TE for pulmonary and aortic valve replacements using varying materials, such as decellularized xeno- and allogenic matrix (e.g. small intestine submucosa, SIS) [9–11], *in vitro* cultured and decellularized matrices [12–15], and degradable synthetic polymers [16–19].

With respect to degradable synthetic polymeric valves specifically, Kluin et al. previously demonstrated the proof-of-concept using electrospun polycarbonate-bisurea based valves, which displayed sustained functionality up to 12 months when surgically implanted in the pulmonary position in sheep [16]. In that study, the valves displayed progressive and heterogenous resorption of the synthetic scaffold material, accompanied with endogenous recellularization and neotissue formation from 6 months on. Tissue formation was reported to develop both within the porous scaffold material and in the form of pannus overgrowth covering the luminal surfaces of the valve leaflets. In addition, feasibility of transcatheter delivery of these valves was shown [16]. Using a similar approach, Bennink et al. reported on the successful application of a resorbable supramolecular elastomeric valved conduit in the pulmonary position in sheep [17]. Recently, the first report on ongoing clinical trials using these valves has been published, showing highly promising results when applied as pulmonary valved conduits for right ventricular outflow tract reconstruction in pediatric patients [20].

Although these results are encouraging, unexplained and uncontrolled adverse remodeling events such as loss of valve function, due to valve thickening and shortening, have been reported in subsets of valves in preclinical studies (reviewed in [7]). For example, Uiterwijk and Smits et al. recently reported on the unexpected and uncontrolled *in situ* remodeling of electrospun polycarbonate-based supramolecular elastomeric valves with a predefined fiber alignment [21]. Despite showing sustained 12-month functionality of the valves, the organization of the endogenously formed collagen unexpectedly could not be dictated using a bio-inspired anisotropic alignment of the synthetic scaffold fibers, and the pre-imposed mechanical anisotropy of the scaffolds was lost already after 1 month *in vivo* [21]. Fioretta et al. reported on heterogeneity in key *in situ* remodeling processes, such as cell infiltration, graft resorption and ECM deposition for minimally invasively implanted resorbable synthetic pulmonary valves in sheep, both between valves, as well as between leaflets within the same valve [21,22]. So far, the regulation of the regenerative response in the complex *in vivo* environment remains poorly understood [23], as well as the role of inflammation therein. The reported variabilities in outcome emphasize the need for more in-depth knowledge of the events, kinetics and mechanisms involved in *in situ* TE, in order to achieve effective tissue formation, limit the risk of unpredicted (maladaptive) remodeling and ensure safe clinical translation.

The goal of this study was to map the long-term spatiotemporal processes of polymeric graft resorption, scaffold-induced inflammation and tissue regeneration in resorbable synthetic pulmonary valves in sheep. To that end, in-depth retrospective analysis was performed on explant material of a previously reported preclinical study [17]. In that study, supramolecular elastomeric heart valve grafts (Xeltis Pulmonary Valved Conduits, XPV, Xeltis, Eindhoven, Netherlands) were implanted at the pulmonary position in an ovine model with follow-up time up to 24 months (2 months N=5, 6 months N=5, 12 months N=5, 24 months N=2). The supramolecular materials platform was chosen to allow easy and independent tuning of mechanics and degradation [24]. To reduce leaflet retraction as often reported for TEHVs [25–27], a slow degrading polymer was chosen to provide retraction resistance until sufficient tissue maturation. The valves were designed with minor redundancy in coaptation area to provide robustness to shortening. On a microstructural level, the valves consisted of relatively large fibers (range 4-8 μm) with the aim to facilitate ingrowth of cells and capillaries. It was demonstrated that with this graft design, safety and functionality remained acceptable throughout the follow-up time, and clinical health, blood values and systemic toxicity were not influenced by the device. The grafts were populated by endogenous cells from 2 months on, in both the conduit and the leaflet of the valves. In order to advance the understanding of how recruited cells and cellular interactions guide scaffold resorption and tissue formation *in vivo*, in the present study, grafts from the previous *in vivo* study were analyzed using a comprehensive immunohistochemistry (IHC) antibody panel [28] and Raman microspectroscopy [29,30].

The antibody panel for IHC was previously developed and validated and consists of antibodies to mark inflammatory cells, valvular interstitial cells (VICs), and extracellular matrix components, such as proteoglycans, collagens and elastic fiber-associated proteins [28]. Specifically, we assessed the presence and phenotype of inflammatory and VIC-like cells, paracrine signaling factors, endothelialization and microvascularization, and extracellular matrix components related to collagen and elastin deposition. Complementary to that, Raman microspectroscopy was applied to mea-

sure the local molecular composition of graft material and newly formed tissue in various locations of longitudinal sections of the explanted valves. Spectroscopic techniques are relatively simple, reproducible and nondestructive. Raman microspectroscopy is a vibrational spectroscopic technique that probes a specific chemical bond (or a single functional group), yielding molecular-level information of functional groups, bonding types, and molecular conformation, thus providing specific information about biochemical composition of tissue constituents and their microenvironments [31,32]. Specifically, we applied Raman microspectroscopy on longitudinal sections of the valve explants including conduit and leaflet to assess the local chemical changes in the scaffold materials, indicative of scaffold resorption, as well as the composition and maturation of collagen in different regions of interest of the valved conduit and for various follow-up times (2, 6, 12, and 24 months). The measured trends on the molecular level were correlated to events on the cell and tissue level using IHC analysis, providing new insights into the spatiotemporal events of inflammation, tissue formation and maturation, and scaffold resorption during material-driven *in situ* heart valve tissue engineering.

2. Materials and methods

2.1. Valve design and in vivo study

Explant material originates from a previously performed study (for detailed study design [17]). Briefly, the leaflets of a valved conduit were produced from polycaprolactone-based supramolecular polymer (electrospun polycaprolactone-ureidopyrimidinone; ePCL-UPy), material 1 (fiber diameter 6-8 µm), which were connected to the conduit consisting of polycarbonate-based supramolecular polymer (electrospun polycarbonate-ureidopyrimidinone; ePC-UPy), material 2 (fiber diameter 4-6 µm) (Fig. 1**A**). These fiber diameters were chosen with the aim to facilitate ingrowth of cells and capillaries. Material 2 was designed to be more stiff when compared to material 1, to provide robustness to the conduit, while material 1 was designed to be more flexible and absorb more slowly, to accommodate the mechanical requirements as well as an anticipated slower restoration process for the leaflets. The conduits were implanted in the pulmonary position in adult Swifter sheep (age 2-4 years, weight 60-90 Kg) and the valves were explanted for analysis after 2 months (N=5), 6 months (N=5), 12 months (N=5), and 24 months (N=2) *in vivo*. The animal usage and study design were approved by the Test Facility's Ethical Committee (Medanex Belgium) for compliance with regulations and the Helsinki protocol. Furthermore, animal welfare was in compliance with the Directive 2010/63/ EU.

2.2. Tissue preparation

The right ventricular outflow tract including the pulmonary valve was excised and fixed in 4% neutral buffered formalin solution. The conduit was opened longitudinally and transmural specimens incorporating the leaflets and conduit wall were used for

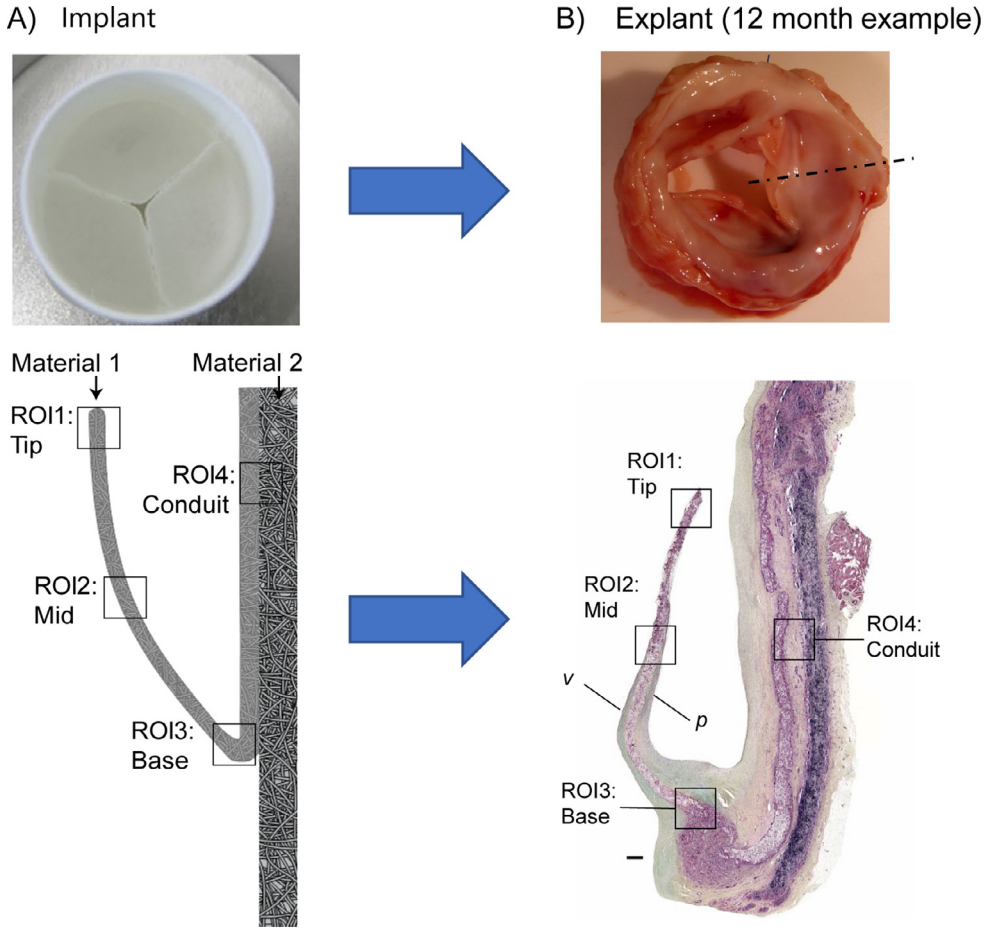

Fig. 1. Overview of valve composition at implantation and explantation. A) Top view of the electrospun valved conduit with schematic longitudinal cross-section, indicating the composite design with material 1 (conduit + leaflet) and material 2 (conduit only), and regions of interest (ROIs) for analysis as indicated. B) Representative example of an explanted valve (12 month example) with gross morphological photograph, indicating cutting plane through the center of the leaflet, resulting in a longitudinal section through both the leaflet and conduit. Displayed is a Movat Pentachrome staining with ROIs for analysis as indicated. P and v indicate the pulmonary and ventricular surfaces of the leaflet, respectively. Photographs and Movat Pentachrome staining are adapted from [17].

further analysis (Fig. 1**B**). The specimens were dehydrated, embedded in paraffin, and sectioned at 4 to 6 µm. Sections were de-paraffinized by washing 3 times 10 min with xylene and rehydrated using a decreasing alcohol series. Subsequently, the sections were washed with deionized water and afterwards phosphate buffered saline (PBS, pH 7.4, Sigma).

2.3. Immunohistochemistry

IHC was performed to evaluate the presence and phenotype of infiltrating inflammatory cells (inducible nitric oxide synthase, iNOS; CD64; CD163; CD44), VIC-like cells (α-smooth muscle actin, αSMA; embryonic form of smooth muscle myosin heavy chain, SMemb; vimentin; calponin), paracrine signaling factors (tumor necrosis factor-α, TNF-α; interleukin-10, IL-10; transforming growth factor-β_1, TGF-β_1), endothelial cells (von Willebrand Factor, vWF), and extracellular matrix components (collagen 1, collagen 3, (tropo)elastin, fibrillin-1, fibrillin-2) (Supplementary Table 1). Antibodies were selected from a previously developed sheep-specific panel [28] and performed on all explant tissues as described. The dilutions and antigen retrieval methods per antibody are specified in Supplementary Table S1 and detailed staining protocol is specified in the Supplementary Methods. Briefly, biotin-labeled secondary antibodies were used and after staining, slides were either treated with SIGMA FAST^{TM} BCIP/NBT (5-Bromo-4-chloro-3-indolulphosphate/Nitro blue tetrazolium, pH 9.5, Sigma) and counterstained with nuclear fast red (Sigma) or treated with LSAB Streptavidin and Nova Red chromogen and counterstained in Hematoxylin. For each stain, an appropriate negative and positive control tissue was selected and included, being either ovine spleen or aortic valve tissue. After dehydration and coverslipping, the stained sections were digitally scanned by CVPath at 20X magnification (CVPath institute Inc, Gaithersburg, US).

2.4. Semi-quantitative analysis of stainings

Semi-quantitative analysis was performed for specified regions of interest (ROIs), i.e. within the graft material of the tip (ROI1), mid (ROI2) and base (ROI3) of the leaflet, the conduit (ROI4) of the pulmonary artery (Fig. 1**A, B**), and the neotissue deposition onto the pulmonary artery. For each stained section, images (1.000.000 µm^2) were selected for the ROI, as well as an image for counterstain reference and background reference using digital analysis software (QuPath) [33]. The ROIs were exported to ImageJ software (NIH, Bethesda, MD, USA) which counted pixel intensities and converted these to a histogram. Based on the intensity of the background and counterstain reference, thresholds were set in order to determine the ranges for positive staining intensity and counterstain intensity. The percentage of positive pixels was then determined by dividing the number of pixels in the positive expression range by the number of pixels in the positive and counterstain region, therefore, excluding background signal and graft material. Data were expressed as boxplots including individual data points using Prism software 5.0 (GraphPad Software, La Jolla, CA). A detailed protocol for the semi-quantitative analysis is specified in the Supplementary methods.

2.5. Raman microspectroscopy

Raman images were acquired from de-paraffinized and rehydrated tissue sections using a Raman microspectroscope (alpha300 R WITec, UIm Germany). Samples were excited using a 532 nm laser and output laser power was 60 mW. Areas of 500 × 500 µm were scanned in the following regions of interest: tip (ROI1), mid (ROI2) and base of the leaflet (ROI3) and the material interface in the conduit (ROI4) (Fig. 1**A, B**). The spectral maps were collected using a line scanning mode (250 lines, 250 points/line, spectral acquisition time=0.05 s/pixel), creating a pixel size of 2 × 2 µm.

2.6. True component analysis and principal component analysis of Raman spectra

Raman spectra represent a highly specific fingerprint, providing molecular information on a sample [34,35]. Multivariate data analysis tools are needed to access the comprehensive information provided by the spectral features and to generate false color-coded intensity distribution heatmaps from hyperspectral imaging maps. Here, we performed True Component Analysis (TCA) to map the location of scaffold components and biological tissue components in each sample. These components were then further analyzed for their molecular composition using Principal Component Analysis (PCA). Specifically, the scaffold material components as identified with TCA were analyzed for chemical changes indicative of scaffold resorption and the biological tissue components were analyzed for collagen formation and maturation.

Image-based data analysis was performed using Project Five Plus Software (WITec, Ulm, Germany). Of each image, data sets were pre-processed using cosmic ray removal and shape background correction. The spectra were cropped (spectral range of 250-3050 cm^{-1}) and normalized to the area of 1. References spectra were measured of both non-implanted graft materials (Xeltis) and biological components, including fibrin (human plasma, sigma Aldrich #F5386), collagen 1 (lyophilized collagen 1 from porcine skin, EPC-elastin products, USA), erythrocytes, and blood components (the latter both extracted from the explant images themselves). All Raman images were analyzed using TCA to identify known biological and graft material components in the recorded explant spectra based on the reference spectra (Supplementary Fig. S1). The pixels that were recognized as similar spectra were assigned to the same spectral component and visualized as intensity distribution heatmaps to localize the different molecular components. Additionally, single point spectra of material and collagen components were extracted and analyzed using principle component analysis (PCA) using Unscrambler X14.2 (Camo, Software, Norway) to investigate molecular differences between the ROIs and between timepoints. The PCA algorithm (NIPALS) allows to decompose the spectral information deciphering spectral similarities and differences into defined vectors – so called principal components (PC). Thereby, PC-1 explains the most influencing spectral signatures, PC-2 the second most relevant information and so on. The PC scores plot can support the visualization of a separation within the dataset. The underlying spectral information is indicated in the corresponding PC loadings plot identifying bands assigned to positive score values as positive peaks and Raman shifts dominating in data with negative score values as negative loadings peaks. PC scores plots and loadings plots were employed to visualize differences of *in vivo* material and collagen spectra at different ROIs and timepoints.

3. Results

3.1. Spatial heterogeneity in inflammatory cell influx with mixed phenotypes

The *in vivo* functionality and general morphological analysis of the valved conduits up to 12 months of implantation has previously been reported by Bennink et al. [17]. In brief, the valves demonstrated sustained functionality *in vivo* up to 12 months follow-up, with mild to moderate regurgitation. Gross morphological analysis showed generally pliable leaflets, with some local anomalies, such as focal leaflet thickening or rolling of the free edge of the leaflet (observed in 6 leaflets of 3 animals). Calcifi-

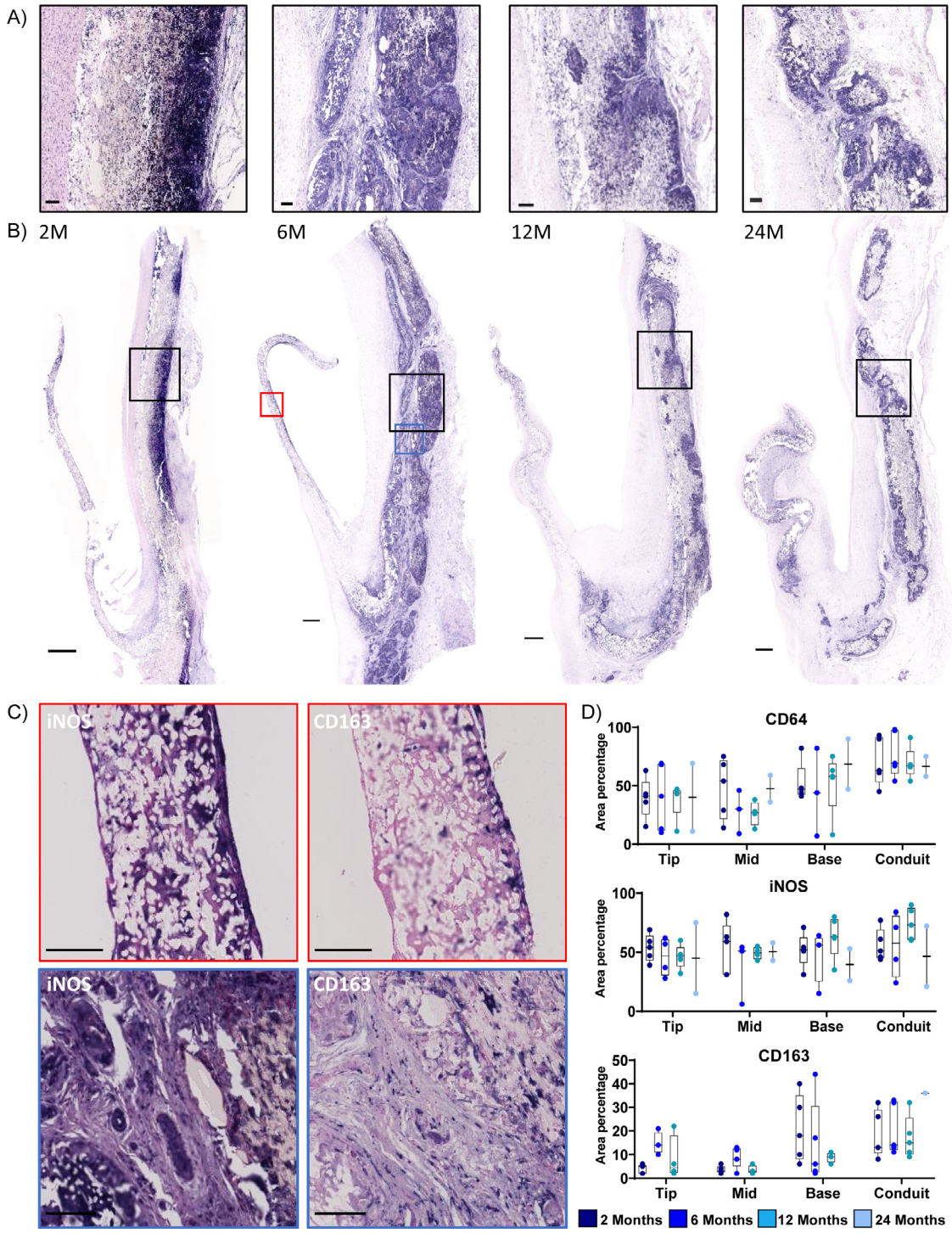

Fig. 2. Macrophage infiltration and polarization over time is region specific. A, B) Representative images of 2, 6, 12, and 24 month explants stained for general macrophage marker CD64, with whole-valve scans and higher magnification images of areas within the graft material of the conduit (location indicated by black boxes) showing that $CD64^+$ macrophages localized within both leaflet and conduit graft material. Positive staining in purple, counterstain in pink. Scale bars, 500 µm for whole-valve scan, 100 µm for zooms. C) Representative images of the pro-inflammatory marker inducible nitric oxide synthase (iNOS) and anti-inflammatory marker CD163 at the mid region of the leaflet (red boxes) and the conduit (blue boxes) of a 6 month explant showing mixed polarization with dominance of pro-inflammatory macrophages within the leaflet graft material and increased anti-inflammatory marker expression within the conduit material. Scale bar, 100 µm. D) Semi-quantification of immunohistochemical stainings (area 100.000 μm^2). N=5 for 2-, 6- and 12 months explants, N=2 for 24 months explants, and N=1 for quantification of the 24 months CD163 staining due to processing artifacts in the CD163 staining of one of the 24 months valves.

cation was reported to be rare with absence of conduit stenosis [17]. The present study extends the depth of analysis of the specimens, including two additional explants with 24 months follow-up, to yield a deeper understanding of the processes involved.

To augment the conventional assessment by tissue morphology of the presence and phenotype of infiltrating inflammatory cells, sections were stained by immunohistochemical methods for the general macrophage marker CD64, as well as the pro- and anti-inflammatory markers iNOS and CD163, respectively, complemented with cytokine stainings for TNF-α, IL-10 and TGF-β_1 (Fig. 2). $CD64^+$ macrophages were detected within the whole leaflet material, as well as the conduit. The distribution was het-

erogeneous with most abundant presence in the base region of the leaflet and in material 2 of the conduit wall, although the extend was variable between explants (Fig. 2**A, B, D**). In the leaflet, less macrophages were detected in the mid region after 6 and 12 months when compared to the base and tip regions. However, an increase was seen in the mid region at 24 months (Fig. 2**D**). Over time, macrophages generally remained present around and within remaining graft material, and macrophage presence diminished with full graft resorption, as was seen for example in the base region of the leaflet after 24 months. Macrophages were mainly present within and close to the graft material. One 2 month explant was exceptional in that respect, displaying erythrocyte-rich matrix in which many macrophages resided within the lumen of the neointima, suggesting that the influx of erythrocytes might be a cue for macrophage recruitment (Supplementary Fig. S2).

In terms of macrophage polarization and general inflammatory state, a mixed inflammatory profile of both pro-inflammatory and anti-inflammatory markers was detected throughout the implantation time within the leaflet base and the conduit (Fig. 2**C,D**). At the tip and mid regions of the leaflet, however, macrophages predominantly expressed iNOS but not CD163 at the 2-month timepoint. After 6 months, anti-inflammatory marker expression increased within the tip of the leaflet, whereas in the mid region this increase was less abundant. Expression of TNF-α and IL-10 generally correlated with the presence of iNOS$^+$ pro- and CD163$^+$ anti-inflammatory macrophages, respectively. Additionally, TGF-β_1 (Supplementary Fig. S3) was mainly detected within graft material in regions with ongoing inflammation.

3.2. Regional heterogeneity in graft resorption correlates with foreign body giant cell formation

Having established the heterogenous influx of inflammatory cells in the conduit and leaflet materials, we then analyzed the extent of graft resorption and tissue formation in the different regions of the valve. To that end, Raman microspectroscopy was performed in the specified regions of interest to acquire the molecular composition in each area. The general local composition of scaffold materials and biological components was determined via TCA. In order to analyze graft resorption per material, the spectra of material 1 and 2 were distinguished from the biological spectra using TCA (Supplementary Fig. S1).

The spectra for material 1 and 2 were analyzed separately and compared to the pre-implant composition of each material using PCA. For the scaffold materials components, spectral changes were mainly dominated by an increasing 1123 cm^{-1} band with implantation duration in both material 1 and 2. The molecular assignment of this band is linked to C-O stretch vibrations and could be linked to an increasing contribution of alkyl-hydroxy groups referring to a degradation of the polymer. The exterior region of the conduit, consisting of material 2, demonstrated major molecular alterations as seen as an increase in the 1123 cm^{-1} band. These spectral changes were already observed after 2 months, indicative of early resorption of material 2, followed by progressive resorption over time (Supplementary Fig. S4). The resorption of material 1 was analyzed per region of interest (Fig. 3). Multivariate analysis of the spectra extracted from the scaffold material maps (Fig. 3**A, B**) and comparison of the average score values for each animal (Fig. 3**C**) demonstrated the most significant variation in the spectral signature arising between non-implanted polymer material and implanted grafts. Corresponding loadings plots depicted the most influencing spectral features (Fig. 3**D**). After 2 months, spectral differences were mainly assigned to intensity differences of the overall polymer spectrum, indicating general erosion of the material rather than molecular changes of the material. Resorption of material 1 after 2 months was most pronounced in the base of the leaflet. 6, 12 and 24 months samples showed alterations in the chemical composition of the polymer with a major influence of an increasing band at 1123 cm^{-1} indicating polymer resorption, which was most pronounced in the conduit region. Most variability in chemical composition amongst explants was present after 2 and 6 months of implantation.

Within the identified areas with most pronounced graft resorption, foreign body giant cells (FBGCs) were present in an inflammatory environment and remained present until full graft resorption, implying a correlation between the presence of FBGCs and graft resorption. In the conduit and leaflet base regions, FBGCs were present already after 2 months (Fig. 4**A**). In the conduit, FBGCs formed predominantly at the outer boundaries of the graft material, rather than inside the graft pores, encapsulating the graft material. In the base region of the leaflet, on the other hand, FBGCs also formed within the pores of the microfibrous graft material (Fig. 4**B**). Substantial variability in the overall number of FBGCs was detected in the conduit and base regions, especially at 2 and 6 months (Fig. 4**A**). Few FBGCs were present in the tip and mid regions of the leaflet at all timepoints, with a slight increase over time. Heterogenous expression of both pro- and anti-inflammatory markers, iNOS and CD163 respectively, were present in FBGCs (Fig. 4**C**).

3.3. VICs transition towards a quiescent phenotype over time

The presence and distribution of tissue producing cells was analyzed by immunohistochemical stainings for αSMA, SMemb and calponin, representing markers for (myo)fibroblast and VIC-like cell activation. At 2 months, many αSMA$^+$, SMemb$^+$, and calponin$^+$ cells were present within the layer of neotissue covering the graft materials, as well as within the microporous graft material at the conduit and base regions specifically (Fig. 5**A,D**). At this time point, SMemb$^+$ and calponin$^+$ cells were also present within the leaflet, whereas no αSMA$^+$ cells were present in the leaflet. At 6 months, αSMA$^+$ cells had migrated towards the tip of the leaflet in most explants (Fig. 5**A**). At 12 and 24 months, the overall presence of VIC-like cells decreased, especially in the graft material and neotissue of the conduit and base regions. Moreover, a strong decrease in overall αSMA expression was observed between 6 and 12 months, indicative of a more quiescent VIC-like phenotype (Fig. 5**D**). However, SMemb expression remained high over time. Vimentin and CD44 expression was minimal in all explant at all time points, with expression restricted to FBGCs within the graft material (Supplementary Fig. S5).

Heterogeneity in tissue deposition as well as presence and morphology of the VICs between explants and the ROIs within one explant was seen (Fig. 5**B, C**). Tissue deposition, and thus tissue thickness, increased with time for all regions within the leaflet, with most variability in the base region. Thickness of the neotissue in the conduit region stabilized after 6 months (Supplementary Fig. S6). The morphology of cells was found to vary depending on the local ECM composition and structure, with elongated cells detected in regions that were rich in fibrillar collagen 1, and rounded cells in regions with more dense, collagen 3-rich matrix (Supplementary Fig. S7). Biglycan and TGF-β_1 expression tended to correlate to calponin and α-SMA expression, suggesting these cells to be predominant producers of these proteins (Supplementary Fig. S7).

3.4. Collagen maturation between 6 and 12 months of implantation with limited elastogenesis

Having established the spatiotemporal patterns in the phenotype of tissue-producing cells, we then assessed the composition and maturation of the endogenously produced tissue. To that end, the fingerprint region of the biological component of the Raman

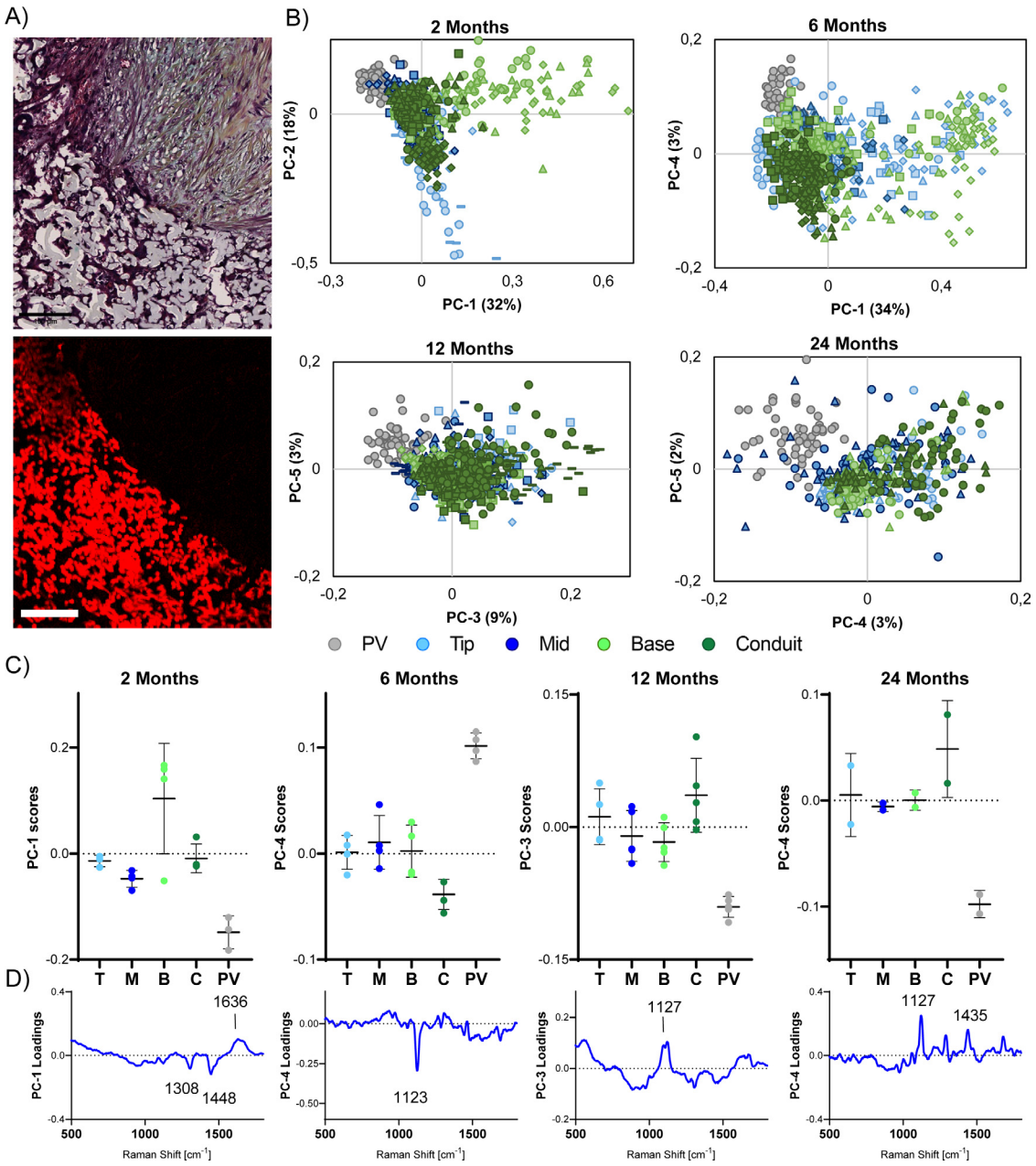

Fig. 3. Raman analysis of *in vivo* resorption of pulmonary valve implant material 1. A) Movat Pentachrome stained base region of a 2 month explant and respective true component analysis (TCA) map of material 1 of this specific region (TCA component of material 1 depicted in red). B) Material 1 spectra were compared for different leaflet regions (ROI1-4) and non-implanted material (PV) after 2, 6, 12, and 24 months using principal component analysis (PCA) scores plot. For each PCA, spectra of the same valve are indicated with the same symbol shape. C) Comparison of ROI-specific average principal component (PC) score values (from B) for each timepoint indicated the biggest discrepancy between implanted and non-implanted material and a tendency towards the strongest resorption in the conduit region. D) Corresponding loadings plots for PCs as indicated. After 2 months, mainly differences in overall polymer signature and intensity were detected. The 6, 12 and 24 month timepoints highlighted a significant band at 1123/1127 cm^{-1} increasing upon polymer resorption.

spectra was analyzed for collagen maturation, in combination with immunohistochemical analysis. Overall, there was progressive tissue deposition in the TEHVs, in the form of pannus formation on the blood-contacting surface of the graft material as well as tissue formation in between the microporous graft fibers as seen in the TCA images (Fig. 6**A**, Supplementary Fig. S8). PCA analysis of the Raman spectra in the tip and mid regions of the leaflet revealed a predominant shift in PC scores between 2 and 6 months, indicating that collagen deposition within the graft material in these regions was mostly detected from 6 months on (Fig. 6**A, B**). The loading plots revealed that changes over time within the leaflet tip and mid regions were dominated by increasing peaks at 860, 940 and 1250 cm^{-1} assigned to the C-C collagen backbone as well as to hydroxyproline, which are mainly linked to overall collagen content (Fig. 6**A, B**). In contrast, the PC scores for the leaflet base and conduit regions showed a more gradual shift between time points, which indicates that collagen was already deposited at 2 months, followed by gradual maturation over time (Fig. 6**C, D**). In the leaflet base, implantation-time dependent findings were observed, with an increasing influence of the amide I band around 1660 cm^{-1}, referring to 3D structural changes due to alterations of α-helix and β-sheet contribution which are present in more stable collagen structures [36] (Fig. 6**C**). The tissue within the conduit indicated slightly different molecular alterations com-

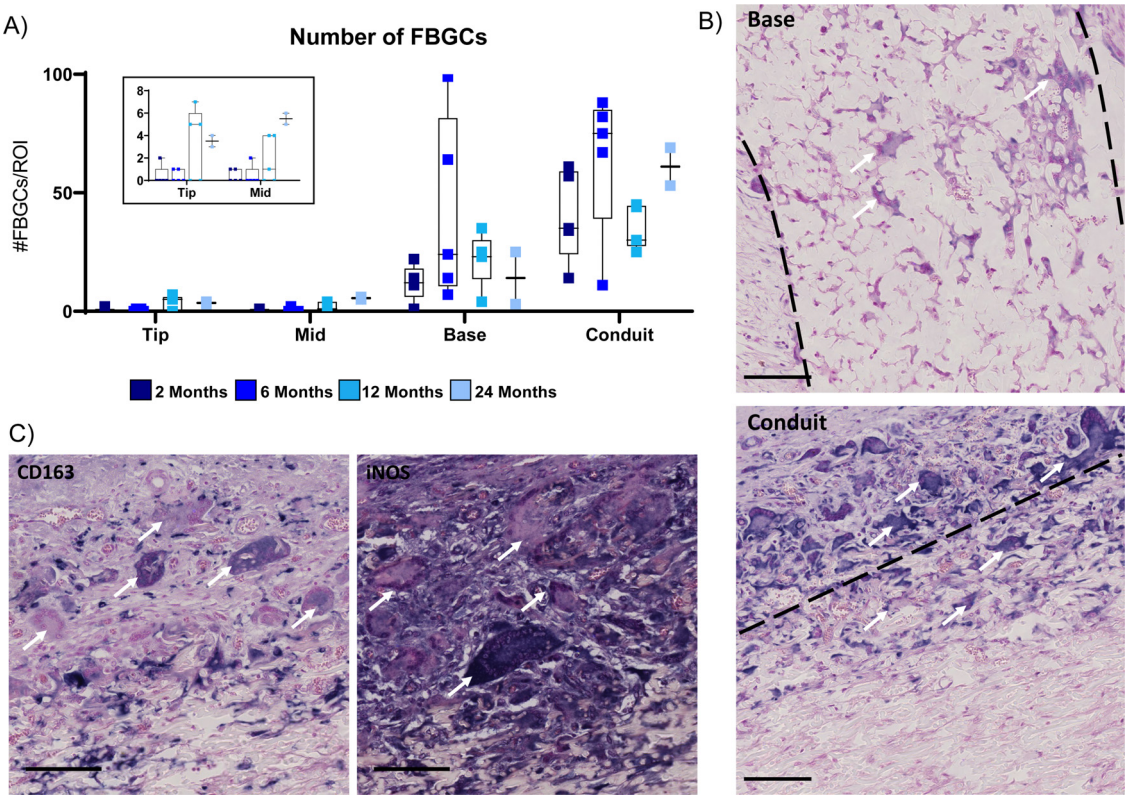

Fig. 4. Overview of foreign body giant cell (FBGC) formation over time. A) FBGCs within each ROI (1,000,000 µm^2) were counted in immunohistochemical images (from CD44 staining), with highest presence in the leaflet base and conduit. B) FBGCs (CD44 staining, positive staining in dark purple), indicated by arrows, within the micropores of the graft material of the base region and the outer layer of the conduit material after 2 months of implantation. Dashed lines indicating the tissue-graft interface. Scale bars, 100 µm. C) Heterogeneity between in pro- and anti-inflammatory marker expression, iNOS and CD163 respectively, in formed FBGCs, indicated by arrows, in the conduit of a 2 month explant. Positive staining in purple, counterstain in pink. Scale bars, 100 µm.

pared to the other regions, with collagen signatures dominated by (hydroxy-)proline at early timepoints, whereas at later timepoints signal intensities assigned to amide I (1664 cm^{-1}) and III (1250 cm^{-1}) as well as the C-C backbone (1450 cm^{-1}) increased (Fig. 6**D**).

To evaluate the extent of collagen maturation specifically, the high wavenumber regions of Raman spectra were analyzed, as shown in Supplementary Fig. S9. A strong shift in the PC scores was detected between 6 and 12 months in the base and mid regions of the leaflet, as well as the conduit. Peaks at 2855, 2877 and 2955 cm^{-1} characteristic for mature collagen type 1 [37] were strongest after 12 and 24 month of implantation in these regions, indicating maturation occurred predominantly between 6 and 12 months. This maturation was confirmed at the protein level by immunohistochemical stainings for collagen type 1 and 3 (Fig. 7**A,B**). Specifically, the immunohistochemical analysis showed a gradual increase in collagen type 1 within the graft material over time (Fig. 7**A**). In addition, a layer of collagenous neotissue was covering the graft material in the conduit region, as well as the base and mid regions of the leaflet (Fig. 7**B**). Tissue deposition on the leaflet tended to occur predominantly on the ventricular side at early time points, progressing from the base region to the mid region of the leaflet. The layers of neotissue were rich in collagen 3 and low in collagen 1 after 2 months of implantation, while over time, collagen 1 expression increased. This was accompanied by the formation of more aligned, fibrous organization, indicating collagen maturation, particularly in the neotissue covering the leaflet (Fig. 7**B**). Within the graft material in the base region, the collagen had a random orientation, while the neotissue at the conduit consisted of more dense collagenous tissue, when compared to the leaflet (Fig. 7**B**).

In addition to collagen fibers, the endogenous formation of a mature elastic fiber network in the valves was assessed. Premature elastic fibers were detected at 24 months, most often located near the conduit region, as well as the leaflet base region, both at the ventricular and pulmonary side (Fig. 8**A**). In all explants, (tropo)elastin was highly expressed within the layer of neotissue (Fig. 8**B**). In some 6- and 12-month valves, fibrillin 2 was expressed within these regions. However, (tropo)elastin expression generally did not colocalize with the microfibrillar proteins fibrillin 1 or 2, both of which are necessary to form mature elastic fibers, as also evident from control staining of native sheep aortic valve tissue (Fig. 8**C**).

3.5. Endothelialization and microvascularization within the microporous graft material

vWF staining was performed to study endothelialization and microvascularization. After 2 months, vWF expression was present at the luminal surface of the neotissue layer deposited on the conduit, with higher expression on the proximal side of the valve compared to the distal side (Supplementary Fig. S10). Sparse expression was detected at the surface of the neotissue layer formed at the base region of the leaflet, predominantly at the pulmonary side and to lesser extent on the ventricular side. After 12 months, the endothelial layer was more pronounced, with expression of vWF on the neotissue of the whole leaflet, on both the pulmonary and ventricular side. From 12 months on, generally, vWF expression could be detected over the entire valve surface. The endothelial cell appearance was similar between earlier and later timepoints, with no clear indications of competition with interstitial cells.

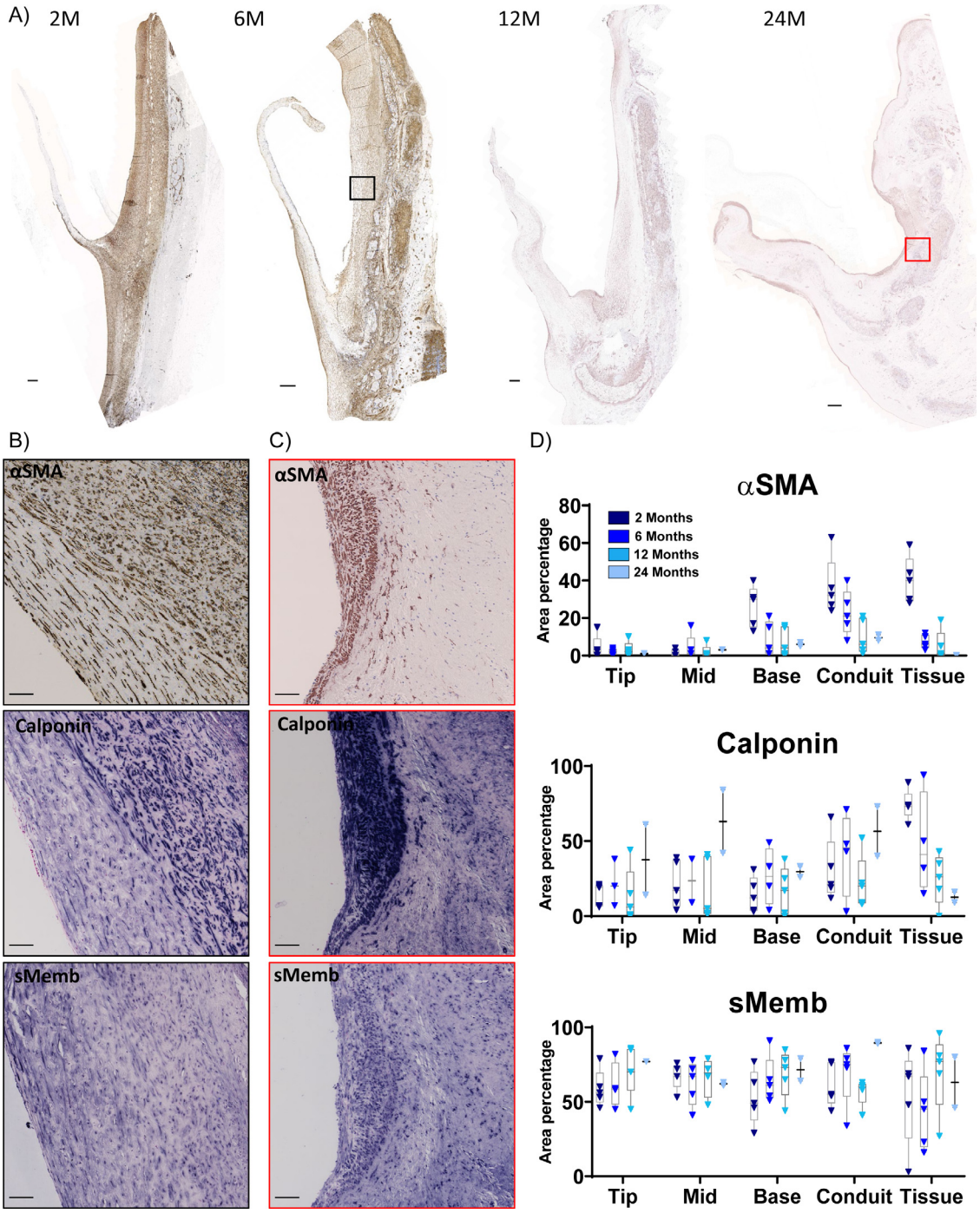

Fig. 5. Valvular interstitial cell (VIC) phenotype shifts towards quiescent state over time. A) Overview of α-smooth muscle actin (αSMA) expression in representative explants at 2, 6, 12, and 24 months. Over time, presence of αSMA^+ cells decreased and remaining αSMA^+ cell localized close to endothelium. Positive staining in brown, nuclei in blue. Scale bars, 500 µm. B) and C) Heterogeneous αSMA, calponin and embryonic smooth muscle myosin heavy chain (SMemb) expression in areas with neotissue deposition onto the conduit after 6 months (B) and 24 months (C) of implantation. Locations indicated with black and red boxes in A. Calponin and Smemb; positive staining in purple, counterstain in pink. Scale bars, 100 µm. D) Semi-quantification of αSMA, calponin and SMemb staining within the leaflet Tip, Mid and Base regions, in the Conduit and in the layer of neotissue deposited onto the graft material in the conduit (Tissue).

Additionally, vWF was detected within and close to the material of the conduit at all time points, indicating the formation of microvasculature within the microporous graft material (Supplementary Fig. S11). In the leaflet, no microvessels were detected within the 2- and 6-months explants. However, the development of microvessels within the leaflet was evident in the 12 months explants, with microvessels formed at the base and mid regions of the leaflet. After 24 months, some microvessels were also present at the tip region of the leaflet. Additionally, larger blood vessels were present within the neotissue layer over the whole leaflet.

4. Discussion

Within this study we aimed to gain more insight into the long-term *in vivo* inflammatory and regenerative processes in *in*

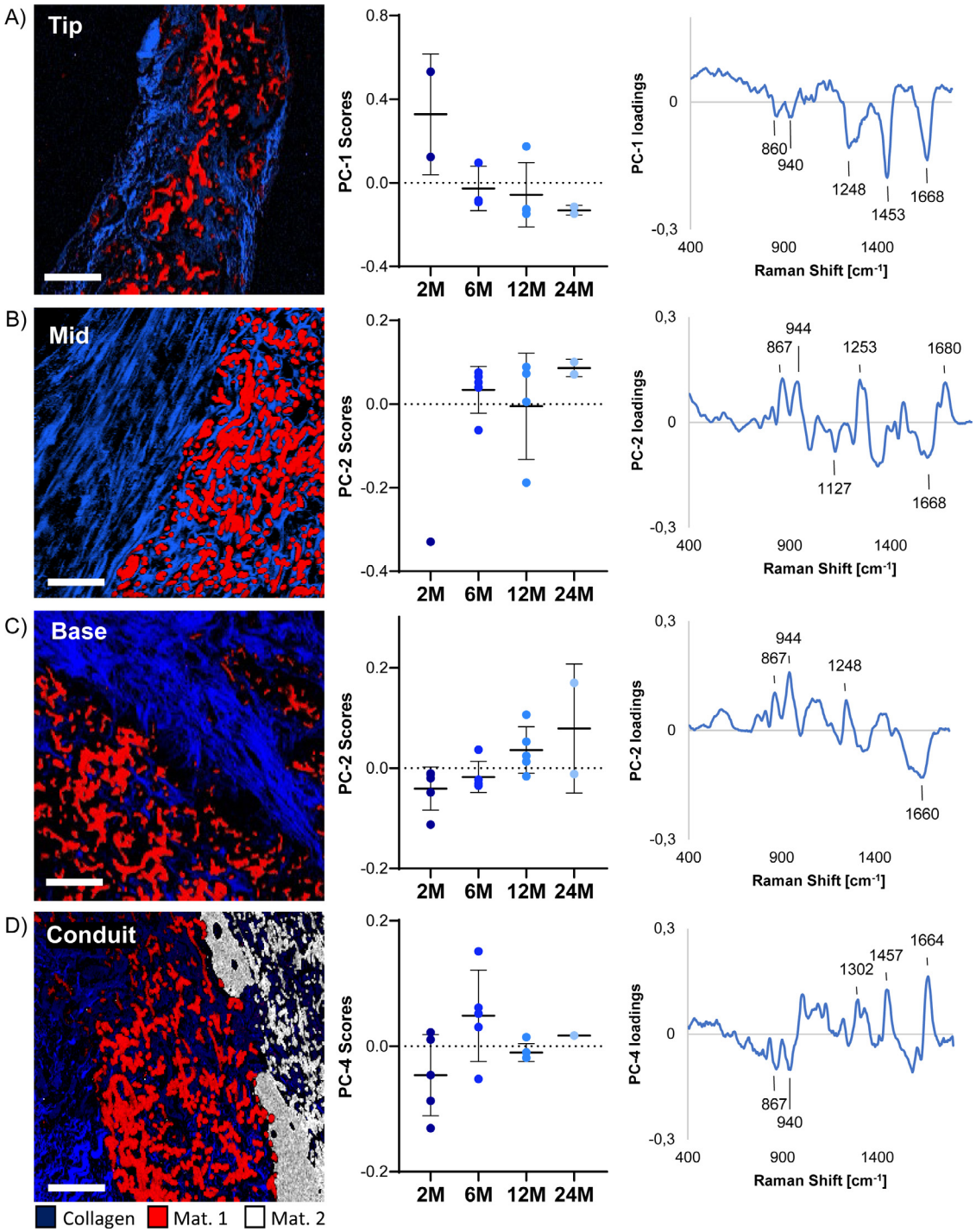

Fig. 6. Raman microspectroscopic analysis of collagen maturation. True Component Analysis (TCA) mapping shows the localization of spectra linked to collagen (blue), material 1 (red) and material 2 (white) for the leaflet tip (A), mid (B), base (C) and conduit (D) regions. Principal Component Analysis (PCA) was performed on the collagen component from the TCA to study collagen maturation with time of implantation. Displayed are the Principal Component (PC) score plots (middle column) and the corresponding loadings plots (right column) for each ROI. Differences in leaflet tip and mid regions were mainly linked to the overall collagen content indicated by bands at 860, 940 and 1250 cm^{-1} assigned to the C-C collagen backbone and hydroxyproline. In the base and conduit additional structural changes related to shifts in the amide I band (1660 cm^{-1}) were observed, indicating collagen maturation.

situ TEHVs based on resorbable supramolecular elastomers. Enabled by a combination of Raman microspectroscopy and IHC, the main findings of this study are that: (1) inflammatory cells, and macrophages in particular, infiltrated the grafts in all regions, with a heterogenous location-dependent phenotype; (2) the resorption of the synthetic graft material was strongly location-dependent, with most rapid resorption in the conduit and leaflet base regions, and correlated with the presence of FBGCs; (3) collagen maturation was effectuated predominantly between 6 and 12 months of implantation, which coincided with a switch to a more quiescent VIC-like phenotype; (4) microvessels formed throughout the microporous graft material, forming a potential source for cell influx. Moreover, substantial valve-to-valve variability in the spatiotemporal distribution of cells, tissue and graft resorption was detected,

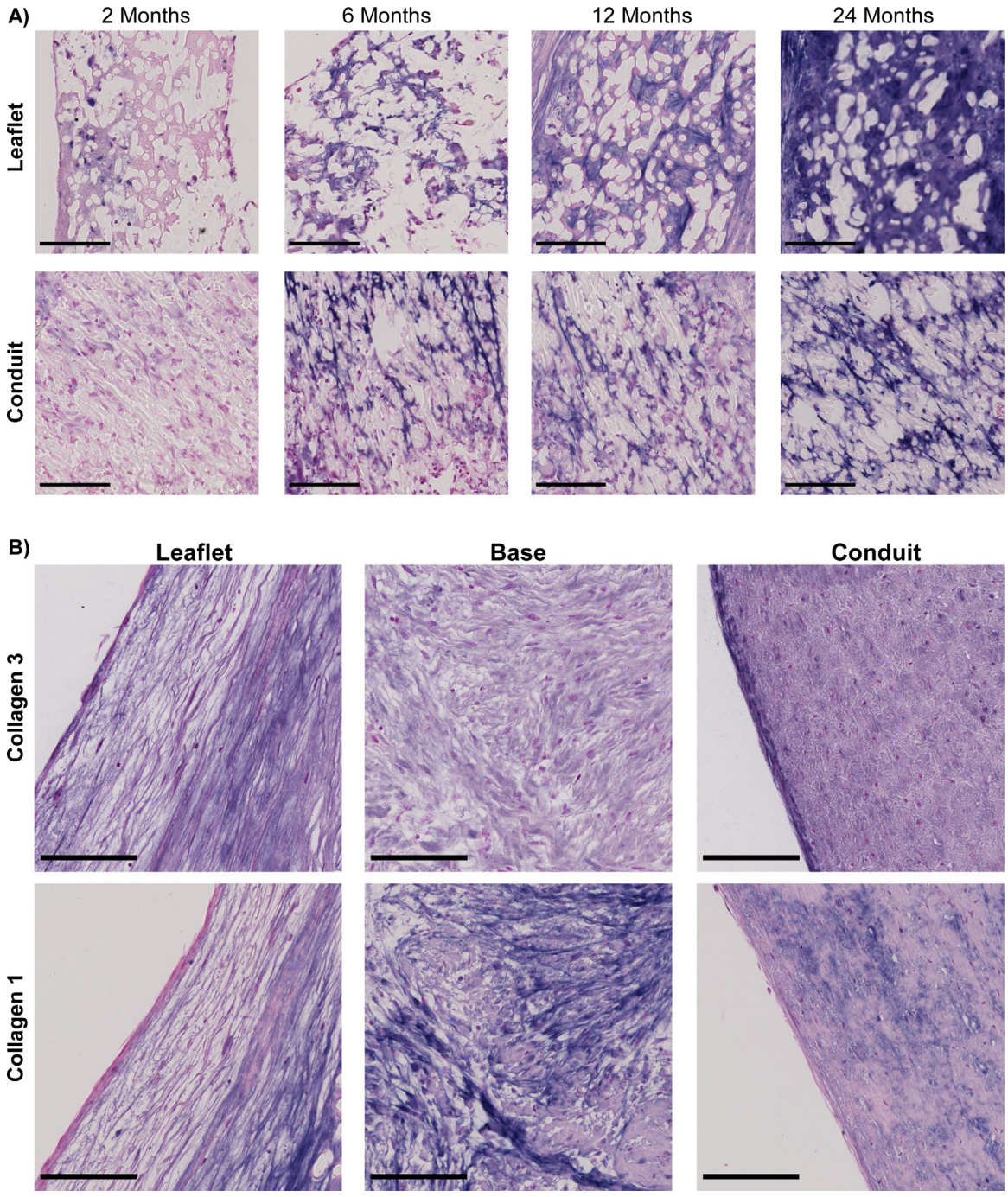

Fig. 7. Spatiotemporal heterogeneity in collagen deposition and maturation. A) Representative images of immunohistochemical staining of Collagen 1 within graft material of the leaflet and conduit. Collagen 1 within the conduit material became more fibrillar over time compared to the leaflet. Scale bars, 100 µm. B) Representative images of collagen 3 and collagen 1, showing variations in composition and organization of collagen in the neotissue of the leaflet, base and conduit after 12 months of implantation. Scale bars, 100 µm. For all images, positive staining in dark purple, counterstain in pink.

with most pronounced variability noted in specimens following implantation of 6 and 12 months. A schematic overview of the key findings is shown in Fig. 9.

One of the most important challenges for *in situ* heart valve tissue engineering, is to maintain the balance between graft resorption and neotissue formation. The mechanical properties of the valve at any time during the regenerative process are determined by the combination of the remnant graft material and the newly formed tissue. Too fast graft resorption (i.e. before sufficient neotissue formation is formed) could lead to mechanical failure (e.g. leaflet tearing). Too slow resorption, on the other hand, could cause a persistent foreign body response, resulting in progressive accumulation of fibrotic tissue, eventually leading to valve stiffening and malfunctioning [38]. Within this study, Raman microspectroscopy analysis uniquely enabled the precise characterization of the local molecular composition of both neotissue and graft material simultaneously in the same location. In heterogeneous samples, such as biological samples, the accuracy of this technique is influenced by the defined spatial resolution. In this study, we used a pixel size of 2 × 2 µm. Thus, the analysis mainly focused on major sample structures such as collagens and the implant material. By combining the Raman data with comprehensive immuno-

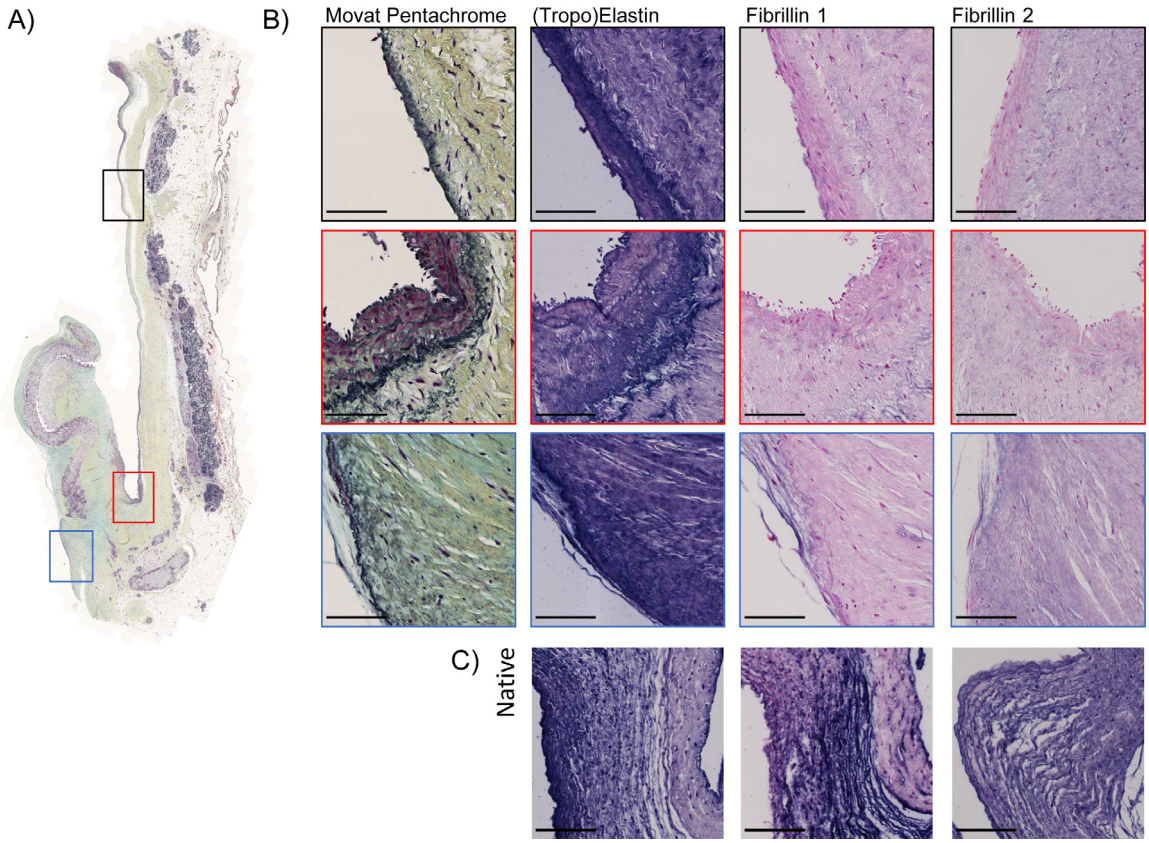

Fig. 8. Elastic fiber network formation in 24 month explant. A) Movat pentachrome staining showing mature elastic fibers in black in a 24 month explant. Elastic fiber network formation mainly occurred near the lumen of the base region (Red and Blue zooms) and conduit (Black zoom). B) Antibody staining of the corresponding regions with (tropo)elastin, fibrillin 1 and fibrillin 2 (positive staining in purple and counterstain in pink), indicating a high expression of (tropo)elastin, but limited fibrillin 1 and fibrillin 2 expression. C) Positive control of the staining on native sheep aortic valve. Scale bars, 100 μm.

histochemical visualization, we were able to correlate the temporal changes in graft resorption and tissue maturation with the local presence of specific cellular populations.

Interestingly, our findings revealed that regions with most pronounced graft resorption, were also the most active regions of tissue formation. At the cellular level, scaffold resorption was associated with the presence of macrophages and FBGCs. This suggests a role for these cells in degrading the synthetic graft material through eliciting reactive oxygen species (ROS) [39,40], although the relative contributions of individual macrophages and FBGCs in graft resorption remain unclear. In addition, these regions were also rich in activated tissue-producing cells that had phenotypic features in common with VICs. Importantly, it was observed that macrophages cleared from regions in which the scaffold had been completely resorbed, thereby preventing a chronic inflammatory environment and chronic presence of activated VIC-like cells. These findings are in line with recent data for vascular grafts suggests that the regenerative response is driven by inflammation [41–43]. Macrophages, in particular, are thought to be instrumental cellular players in the processes of graft resorption and tissue formation as they have a dual function: on the one hand, macrophages govern tissue formation via cross-talk to tissue-producing cells [44–46], while on the other hand, macrophages dictate graft resorption through oxidative and enzymatic pathways [47,48]. Dependent on the mechanism of stimulation, macrophages undergo phenotypic modulation and secrete a variety of paracrine factors by which they regulate the behavior of tissue-producing cells (e.g. differentiation, migration and proliferation) and thus the deposition of new extracellular matrix [44–46,49]. Overall, these findings suggest that macrophages and FBGCs are hinging cell types in maintaining the local balance between graft resorption and tissue formation, thereby safeguarding structural integrity of the valve despite the strong spatial heterogeneities in the rates of tissue formation and graft resorption as observed.

One of the most important findings of this study is the spatial heterogeneity in cellular phenotypes, tissue formation and scaffold resorption. So far, the knowledge on *in situ* heart valve tissue engineering using resorbable synthetic scaffolds has been largely speculative and predominantly based on studies on *in situ* tissue-engineered vascular grafts, which have a less complex geometry and hemodynamic environment. The spatial variability as observed may be explained by: (1) the different sources and rates of cell influx in the different regions, and (2) an influence of the local hemodynamic loads. With respect to the former, the exact source and routes of cellular influx could not be identified from this retrospective study, and are topic of active investigation. In previous studies on valvular and vascular grafts, three main routes of cellularization have been identified: (i) (early) influx of circulatory cells [25,50], (ii) tissue overgrowth originating from the native arterial wall [16,22], and (iii) transmural ingrowth of inflammatory cells and microvasculature [26,51,52]. Within the present study, all three routes seemed to play a role in the regenerative process. After 2 months, macrophages, predominantly of a pro-inflammatory phenotype, were present within the leaflet especially near the tip, suggesting a likely origin from the circulation. Correspondingly, rapid cellularization of the leaflets of acellular valvular implants has been previously reported already 5 h [25] and 15 h [50] post-implantation, proposing that these cells originate from the blood. Tissue formation at later time-points was observed both in between scaffold fibers, as well as deposited on the luminal surfaces,

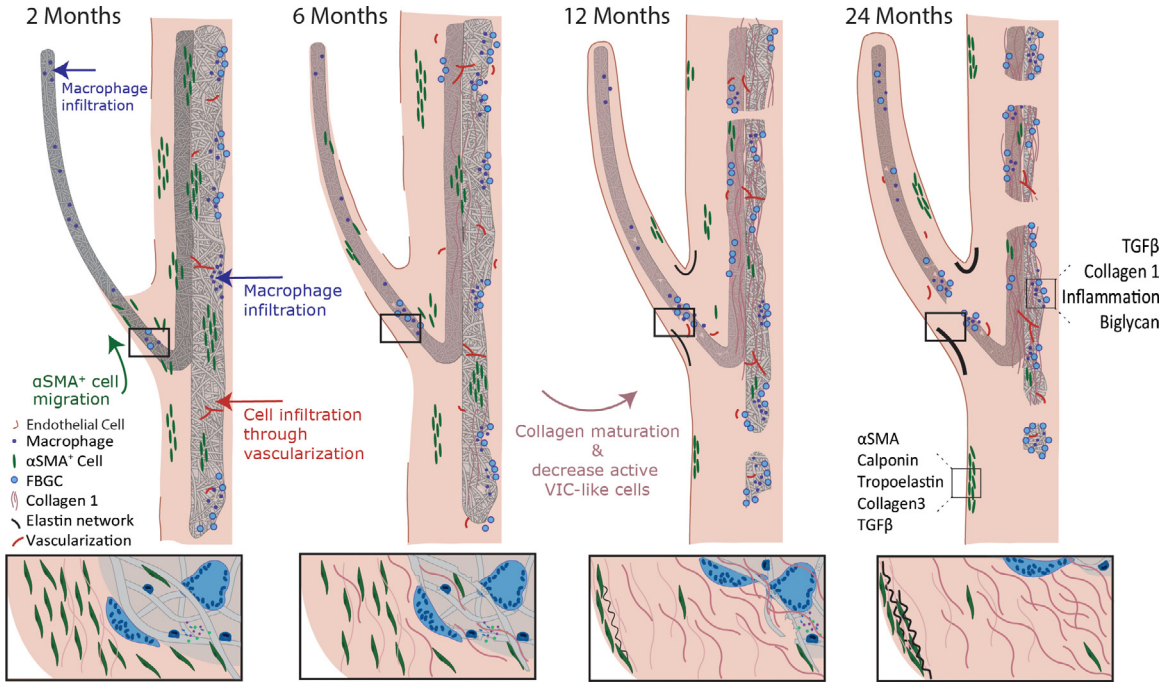

Fig. 9. Schematic overview of essential processes involved in *in situ* heart valve regeneration. After 2 months, macrophages had infiltrated the graft material of both the leaflet and conduit. In the conduit, a microvasculature was already forming, providing an additional cell source. αSMA$^+$ cells migrated from the conduit towards the tip of the leaflet over time, depositing collagen 3-rich tissue. The deposited collagenous tissue became more mature through 6-12 months, accompanied by a decrease in αSMA$^+$ cells within this timeframe. Graft resorption was most pronounced in the leaflet base and conduit correlating with a high presence of FBGCs in an inflammatory environment, eventually causing successive resorption within these regions after 24 months. Inflammation had resolved in regions with complete graft resorption. Areas with ongoing inflammation were high in TGF-β_1, collagen 1 and biglycan. Areas in which αSMA$^+$ cells localized underneath the endothelium were high in calponin$^+$ cells, (tropo)elastin, collagen 3 and TGF-β_1. Zooms indicate the regenerative process over time within the leaflet base region specifically. After 2 months, macrophage and VIC-like cell infiltration and FBGC formation was observed. Between 6 and 12 months of implantation, tissue deposition and graft resorption increased, with enhanced tissue maturation and decreased presence of activated VIC-like cells. Additionally, from 12 months onwards elastic fiber formation was seen in the neotissue within this region. After 24 months, complete graft resorption was accompanied with resolution of inflammation within the leaflet base region.

progressing from the leaflet base. Within the conduit, immune cell infiltration occurred most probably through transmural migration and neovascularization. Interestingly, calponin and SMemb positive cells were present within leaflet after 2 months, whereas αSMA$^+$ cells were not found within the leaflet material but seemed to migrate from the neotissue of the wall over the leaflet material with time, accompanied by tissue deposition from the wall to the leaflet tip with time. The exact origin of the tissue-producing cells remains unknown, however these results suggest that, similar to the infiltrating immune cells, these cells originate from various sources and from various precursor cells. In this respect, interesting phenomena were observed in the neotissue layers near the lumen, with progressively more αSMA and calponin positive cells present directly underneath the endothelium. This correlated with high levels of TGF-β and biglycan and deposition of collagen 3, which could indicate endothelium-to-mesenchymal transition (EndMT) [53,54]. It is known that VEC-VIC interaction is very important for valve homeostasis. In adult valves, limited EndMT is taking place, and this process can contribute to replenish the VIC population as part of physiological valve remodeling [53]. However, increased EndMT in adult valves is often associated with pathological remodeling [55]. For the analyzed explants, it remains debatable whether the process of EndMT is in fact ongoing, and if so, if it is leading to pathological remodeling or is simply part of the necessary wound healing response for example as an additional source of tissue producing cells. When studying cellularization routes, it must be stressed that biases in the animal model should be considered when translating optimal graft design towards human application. Tissue overgrowth is suggested to be more excessive within the ovine model when compared to humans and typically, native ovine leaflets have a higher cellularity, more defined valvular layers and a lower amount of elastin [28,56]. Moreover, Dekker et al. recently demonstrated that healthy native ovine valves display a higher expression of activated VICs when compared to human valves [28].

In addition to differences in cell influx, the spatial patterns in inflammation and tissue formation also suggest an important role for the heterogeneous local hemodynamic loads, as for example the leaflet base region is exposed to high strains and different shear stress profiles when compared to the conduit. Shear stresses have been shown to play a dominant influence on the recruitment of monocytes to electrospun scaffolds [57,58]. In addition, both macrophages and tissue-producing cells, such as (myo)fibroblasts and VICs, are known to be highly mechanosensitive [59,60]. *In vitro* studies have demonstrated cyclic strain to influence macrophage polarization [61,62]. Moreover, cyclic strain decreased degradative activity of macrophages within a biomaterial [62]. Additionally, both cyclic stretch and shear stress influence the cross-talk between (myo)fibroblasts and macrophages, and by that affecting tissue deposition [63]. Recent *in vivo* studies have shown the importance of hemodynamics in inflammation-driven *in situ* tissue regeneration of vascular grafts [64–66] and valves [14]. Moreover, in accordance with the present findings, Motta et al. recently reported on the importance of hemodynamic loads, in particular cyclic stretch, on the inflammation and *in situ* regeneration of de novo engineered extracellular matrix-based TEHVs [67]. In order to enable better prediction of *in situ* (mal)adaptive remodeling, hypothesis-driven studies have been focusing on macrophage and tissue-producing cell behavior and the influence of their microenvironment such as graft design (e.g. porosity, surface chemistry), as well as mechanical loading [14,21,60,63,66,68,69].

Interestingly, the FBGC formation in the conduit region tended to localize around the outer boundaries of the graft material, rather than within the pores of the highly porous graft material as was observed in the leaflet material. This difference may be a consequence of the differences in hemodynamics between the moving leaflet versus the static conduit wall. Alternatively, subtle differences in microstructure, e.g. fiber diameter (material 1: 6-8 μm, material 2: 4-6 μm) and pore size, between leaflet material 1 and conduit material 2 may have played a role. Fiber diameter and pore size are design parameters known to influence cell infiltration and fibroblast activation, as well as macrophage polarization [68,70,71]. Generally, a relatively large fiber diameter (in the range of several micrometers) and pore size facilitates cell influx and induces a more favorable inflammatory response, characterized for example by a favorable M2/M1 macrophage ratio, when compared to small-fiber (< 1 μm) scaffolds [72,73]. Moreover, Wissing et al. previously showed that resorption of microfibrous scaffolds by macrophages is dependent on the scaffold microstructure [40]. *In vitro* FBGC formation is known to be regulated by multiple factors, such as cell density, material chemistry and structure, and interleukin-4 (IL-4) stimulation, with the latter being recently suggested to be most important [39,74,75]. In the leaflet base and conduit regions more transmural migration of macrophages is occurring and more M2 macrophages, known to secrete IL-4, are present alongside iNOS positive macrophages, when compared to the mid and tip region of the leaflet. Possibly, this contributes to a higher presence of FBGCs in the base and wall region.

With respect to the temporal process of tissue formation and maturation, *in situ* tissue engineering has been postulated to mirror the wound healing cascade [5]. Interestingly, Raman TCA analysis suggested the presence of fibrin-like tissue, tightly surrounding the synthetic graft fibers, in both graft materials at all timepoints (Supplementary Fig. S12). Within these regions, erythrocytes and overlap with blood components could also be detected, both inside graft material and the neotissue surrounding the graft material. It is interesting to further define this structure, as fibrin is thought to be deposited as part of the early host response [76] and to serve as a template for new tissue formation similar to the preliminary matrix in physiological wound healing [77]. Importantly, we detected that collagen maturation developed mainly between 6 and 12 months after implantation. The immunohistochemical stainings revealed a transition from a more collagen 3 to a more collagen 1 dominated tissue, which is similar to physiological wound healing. Notably, the maturation of the tissue was accompanied by a switch in the phenotype of the VIC-like cells to a more quiescent αSMA$^-$ phenotype. Possibly this switch was facilitated by changes in the local inflammatory environment. In healthy adult valves mainly quiescent VICs, marked by e.g. vimentin, reside within the leaflet [78,79], with subpopulations of smooth muscle cells and myofibroblasts [78,80]. Surprisingly, vimentin positive cells infiltrated only very sparsely in the explants, whereas in the native sheep aortic valve used as positive control, many cells expressing vimentin were present. It is unclear what the cause of this lack of vimentin expression is. Especially at early timepoints, αSMA and calponin positive cells were abundantly present within the explants. The presence of these activated fibroblasts is typically associated with pathological remodeling and excess tissue deposition [81]. However, for *in situ* TE these cells are essential to facilitate endogenous tissue deposition. We believe it is essential that over time these cells return to their quiescent state to prevent fibrosis and leaflet contraction, as previously seen in many *in vitro* tissue-engineered heart valves [27,82]. The marked decrease in the presence of αSMA and calponin positive cells over time, accompanied with the maturation of the tissue and the resorption of the scaffolds, indeed suggests that the regenerative response in the explants was moving towards a state of tissue homeostasis, rather than pathological remodeling. However, longer follow-up times are warranted to investigate the functionality and composition of the valves upon complete resorption of the graft materials.

The formation of elastic fibers was detected only at late timepoints, with mature elastic fibers mainly detected after 24 months of implantation. In native heart valves, the elastin network is formed at the very early life stages and remains functional throughout a lifetime, with little to no new elastin formation [83]. Similar to previous studies, sparse mature elastic fiber formation was detected, although not yet comparable to the native elastic fiber network [16,84]. In all valves, (tropo)elastin was extensively produced, whereas the expression of the microfibrillar network protein fibrillin 1 and fibrillin 2 was very sparsely detected. This suggests that the bottleneck for new elastic fiber formation might not be the production of tropoelastin and the formation of elastin as such, but rather the presence and/or assembly of network proteins. We speculate that the abundant presence of inflammatory cells leads to a proteolytic environment of elastases and matrix metalloproteinases (MMPs) that may inhibit elastogenesis [85]. This may also explain why elastic fiber assembly was only detected at late time points, at which the inflammatory environment had locally resolved in graft-free regions. The latter was recently reported by Duijvelshoff et al., who demonstrated a trend of mature elastic fiber regeneration in resorbable synthetic endovascular stents in pace with a reduction in macrophage presence [86].

Finally, even within this very homologous test group of healthy, young sheep, variability was seen between explants of each time point. Most variability in tissue formation, as well as inflammation and graft resorption, between the valves tended to occur in the first 6 months. Within this timeframe, many processes are ongoing, influencing the timing and extend of other processes involved in endogenous tissue regenerative cascade. Potential sources of variability might be minor variabilities in the surgical procedure at implantation or through differences in host immunological state [8]. Reasonably, more variation can be expected when translating towards more heterogenous patient populations [87].

The findings of the present study provide several important indications for future clinical translation. Overall, the present findings regarding tissue formation and maturation suggest that scaffold resorption of *in situ* TEHVs should be relatively slow to allow for sufficient mature and functional tissue formation prior to full scaffold resorption. Perhaps more importantly, the scaffold design should facilitate maintenance of the balance between resorption and tissue formation by the cells in order to deal with spatial heterogeneities that are observed in the complex heart valve geometry. Appropriate microstructural and mechanical design is key in that respect, where the microstructure should be chosen with sufficient pore size for ingrowth of cells and capillaries, and spatiotemporal heterogeneity between the conduit and leaflet regions in particular should be considered. It should be emphasized that some of the current findings may be specific to the sheep model, and may occur differently in patients. From a translational point-of-view patient-centered research is essential [88]. These considerations may become even more important when translating to the aortic position due to the more stringent, less-forgiving hemodynamic environment. Moreover, given that aortic valves are mostly implanted in adult or elderly patients, stronger inter-patient variability is to be anticipated. Patient-specific sources of variability for this patient population are proposed to include co-morbidities, such as diabetes, and sex- and age-related changes, medications and environmental factors [8,87,89]. Dedicated research is necessary to determine if patient-specific graft design is necessary and how immunomodulatory graft design should be optimized to ensure safe and robust clinical translation to various patient populations.

Limitations

This study has several limitations. One important limitation is that this was a retrospective study and only endpoint data measurements were used in this study. Therefore, it remains speculative which early events could have led to certain downstream remodeling. Spectral analysis of Raman data was performed only within the graft material. As longitudinal analysis of a single valve was not possible, variability between selected areas could occur due to resorption of graft material, especially in the base region, causing variability in outcome. Moreover, local scaffold resorption could not be reliably quantified as resorption of supramolecular polymers is a complex process with multiple potential functional implications (e.g. fiber swelling, changing mechanical properties [47,90]) which is challenging to measure in explant material. Qualitative analysis of scaffold resorption by SEM (e.g. in terms of fiber cleavage, erosion) as previously described [16,21] could not be performed with the samples available. Additionally, intense signal and close material interactions, such as fibrin, might cause noise in the spectrum. A more detailed pixel size could be used to overcome this limitation, however, here we opted for compromising on the minimal pixel size in order to enable scanning of various larger regions within the valve. Another limitation of this study is the limited sample size. However, there are only few studies on long-term *in vivo* implantations of resorbable synthetic heart valves available to date, so despite the limited sample numbers, the presented information represents a valuable contribution to our understanding of *in situ* heart valve tissue engineering.

Conclusion

With these analyses, we uncovered new insights in the endogenous tissue restoration response regarding infiltration and presence of immune cells and tissue forming cells and their correlation to graft resorption and neotissue formation and maturation over time. Our findings show important spatial heterogeneities in the regenerative process, most likely as the combined effect of heterogeneous cellular repopulation mechanisms and heterogeneity in the local hemodynamic loads, which may fuel the rational design of improved grafts. To fully understand the *in situ* regenerative response, more in-depth, comprehensive *in vivo* analysis and mechanistic *in vitro* work with focus on the role of proposed regulators of regeneration including inflammation, local extracellular matrix, graft design, and especially local hemodynamics and the downstream effects thereof are warranted. However, to ensure robust clinical translation, a holistic approach is needed, focusing not only on the graft properties, but also on implant-independent, patient-specific factors.

CRediT author statement

Bente de Kort: Investigation, Formal Analysis, Data curation, Visualization, Writing–Original Draft; **Julia Marzi**: Investigation, Formal analysis, Visualization, Writing-Review & Editing; **Eva Brauchle**: Investigation, Formal analysis; **Arturo Lichauco**: Software, Validation; **Hannah Bauer**: Validation, Writing-Review & Editing; **Aurelie Serrero**: Resources, Writing-Review & Editing; **Sylvia Dekker**: Resources, Validation; **Martijn Cox**: Conceptualization, Resources, Writing-Review & Editing; **Fred Schoen**: Validation, Writing-Review & Editing; **Katja Schenke-Layland**: Resources, Writing-Review & Editing; **Carlijn Bouten**: Writing-Review & Editing, Funding acquisition; **Anthal Smits**: Conceptualization, Formal Analysis, Writing–Original Draft & Editing, Funding acquisition, Supervision.

Funding

This research was financially supported by the Gravitation Program “Materials Driven Regeneration”, funded by the Netherlands Organization for Scientific Research (024.003.013), and a Career Acceleration and Development Grant to A. Smits by the CardioVascular Research Netherlands (CVON) 1Valve consortium. The collaboration between Eindhoven University of Technology and the University of Tübingen for the Raman microspectroscopy analysis was facilitated by a Short-Term Fellowship (8169) of the European Molecular Biology Organization (EMBO) to A. Smits. This study was financially supported by the Ministry of Science, Research and the Arts of Baden-Württemberg (33-729.55-3/214 and SI-BW 01222-91 to K.S.-L.) and the Deutsche Forschungsgemeinschaft (INST 2388/64-1 to K.S.-L.).

Declaration of Competing Interest

The research labs from K. Schenke-Layland and A. Smits performed independent scientific contract work for the company Xeltis and received for this work financial compensation. M. Cox, H. Bauer and A. Serrero are employees of Xeltis, M. Cox and C. Bouten are shareholders of Xeltis and F. Schoen is a financially compensated scientific advisor to Xeltis. All other authors report no competing interests.

Supplementary materials

Supplementary material associated with this article can be found, in the online version, at doi:10.1016/j.actbio.2021.09.005.

References

[1] S.H. Rahimtoola, Choice of prosthetic heart valve in adults. An update, J. Am. Coll. Cardiol. 55 (2010) 2413–2426, doi:10.1016/j.jacc.2009.10.085.
[2] P. Bloomfield, D.J. Wheatley, R.J. Prescott, H.C. Miller, Twelve-year comparison of a Bjork-Shiley mechanical heart valve with porcine bioprostheses, N. Engl. J. Med. 324 (1991) 573–579, doi:10.1056/NEJM199102283240901.
[3] K. Hammermeister, G.K. Sethi, W.G. Henderson, F.L. Grover, C. Oprian, S.H. Rahimtoola, Outcomes 15 years after valve replacement with a mechanical versus a bioprosthetic valve–Final report of the Veterans Affairs randomized trial, J. Am. Coll. Cardiol. 36 (2000) 1152–1158, doi:10.1016/S0735-1097(00)00834-2.
[4] T. Bourguignon, A.L. Bouquiaux-Stablo, P. Candolfi, A. Mirza, C. Loardi, M.A. May, R. El-Khoury, M. Marchand, M. Aupart, Very long-term outcomes of the carpentier-edwards perimount valve in aortic position, Ann. Thorac. Surg. 99 (2015) 831–837, doi:10.1016/j.athoracsur.2014.09.030.
[5] T.B. Wissing, V. Bonito, C.V.C. Bouten, A.I.P.M. Smits, Biomaterial-driven *in situ* cardiovascular tissue engineering–A multi-disciplinary perspective, Npj Regen. Med. 2 (2017) 18, doi:10.1038/s41536-017-0023-2.
[6] C.V.C. Bouten, A.I.P.M. Smits, F.P.T. Baaijens, Can we grow valves inside the heart? Perspective on material-based *in situ* heart valve tissue engineering, Front. Cardiovasc. Med. 5 (2018) 54, doi:10.3389/fcvm.2018.00054.
[7] E.S. Fioretta, S.E. Motta, V. Lintas, S. Loerakker, K.K. Parker, F.P.T. Baaijens, V. Falk, S.P. Hoerstrup, M.Y. Emmert, Next-generation tissue-engineered heart valves with repair, remodeling and regeneration capacity, Nat. Rev. Cardiol. 18 (2021) 92–116, doi:10.1038/s41569-020-0422-8.
[8] A.I.P.M. Smits, C.V.C. Bouten, Tissue engineering meets immunoengineering–Prospective on personalized *in situ* tissue engineering strategies, Curr. Opin. Biomed. Eng. 6 (2018) 17–26, doi:10.1016/j.cobme.2018.02.006.
[9] J.W. van Rijswijk, H. Talacua, K. Mulder, G.P.J. van Hout, C.V.C. Bouten, P.F. Gründeman, J. Kluin, Failure of decellularized porcine small intestinal submucosa as a heart valved conduit, J. Thorac. Cardiovasc. Surg. 160 (2020) e201–e215, doi:10.1016/j.jtcvs.2019.09.164.
[10] T. Goecke, K. Theodoridis, I. Tudorache, A. Ciubotaru, S. Cebotari, R. Ramm, K. Höffler, S. Sarikouch, A. Vásquez Rivera, A. Haverich, W.F. Wolkers, A. Hilfiker, *In vivo* performance of freeze-dried decellularized pulmonary heart valve allo- and xenografts orthotopically implanted into juvenile sheep, Acta Biomater. 68 (2018) 41–52, doi:10.1016/j.actbio.2017.11.041.
[11] R. Ramm, T. Goecke, K. Theodoridis, K. Hoeffler, S. Sarikouch, K. Findeisen, A. Ciubotaru, S. Cebotari, I. Tudorache, A. Haverich, A. Hilfiker, Decellularization combined with enzymatic removal of N-linked glycans and residual DNA reduces inflammatory response and improves performance of porcine xenogeneic pulmonary heart valves in an ovine *in vivo* model, Xenotransplantation 27 (2020) 1–12, doi:10.1111/xen.12571.

[12] S.E. Motta, V. Lintas, E.S. Fioretta, P.E. Dijkman, M. Putti, E. Caliskan, H. Rodriguez Cetina Biefer, M. Lipiski, M. Sauer, N. Cesarovic, S.P. Hoerstrup, M.Y. Emmert, Human cell-derived tissue-engineered heart valve with integrated Valsalva sinuses–Towards native-like transcatheter pulmonary valve replacements, Npj Regen. Med. 4 (2019) 14, doi:10.1038/s41536-019-0077-4.
[13] V. Lintas, E.S. Fioretta, S.E. Motta, P.E. Dijkman, M. Pensalfini, E. Mazza, E. Caliskan, H. Rodriguez, M. Lipiski, M. Sauer, N. Cesarovic, S.P. Hoerstrup, M.Y. Emmert, Development of a novel human cell-derived tissue-engineered heart valve for transcatheter aortic valve replacement: an *in vitro* and *in vivo* feasibility study, J. Cardiovasc. Transl. Res. 11 (2018) 470–482, doi:10.1007/s12265-018-9821-1.
[14] M.Y. Emmert, B.A. Schmitt, S. Loerakker, B. Sanders, H. Spriestersbach, E.S. Fioretta, L. Bruder, K. Brakmann, S.E. Motta, V. Lintas, P.E. Dijkman, L. Frese, F. Berger, F.P.T. Baaijens, S.P. Hoerstrup, Computational modeling guides tissue-engineered heart valve design for long-term *in vivo* performance in a translational sheep model, Sci. Transl. Med. 10 (440) (2018), doi:10.1126/scitranslmed.aan4587.
[15] J. Reimer, Z. Syedain, B. Haynie, M. Lahti, J. Berry, R. Tranquillo, Implantation of a tissue-engineered tubular heart valve in growing lambs, Ann. Biomed. Eng. 45 (2017) 439–451, doi:10.1007/s10439-016-1605-7.
[16] J. Kluin, H. Talacua, A.I.P.M. Smits, M.Y. Emmert, M.C.P. Brugmans, E.S. Fioretta, P.E. Dijkman, S.H.M. Söntjens, R. Duijvelshoff, S. Dekker, M.W.J.T. Janssen-van den Broek, V. Lintas, A. Vink, S.P. Hoerstrup, H.M. Janssen, P.Y.W. Dankers, F.P.T. Baaijens, C.V.C. Bouten, *In situ* heart valve tissue engineering using a bioresorbable elastomeric implant–From material design to 12 months follow-up in sheep, Biomater. 125 (2017) 101–117, doi:10.1016/j.biomaterials.2017.02.007.
[17] G. Bennink, S. Torii, M. Brugmans, M. Cox, O. Svanidze, E. Ladich, T. Carrel, R. Virmani, A novel restorative pulmonary valved conduit in a chronic sheep model–Mid-term hemodynamic function and histologic assessment, J. Thorac. Cardiovasc. Surg. 155 (2018) 2591–2601 e3, doi:10.1016/j.jtcvs.2017.12.046.
[18] Y. Miyazaki, O.I. Soliman, M. Abdelghani, A. Katsikis, C. Naz, S. Lopes, B. Warnack, M. Cox, Y. Onuma, P.W. Serruys, Acute performance of a novel restorative transcatheter aortic valve–Preclinical results, EuroIntervention 13 (2017) e1410–e1417, doi:10.4244/EIJ-D-17-00554.
[19] G.N. Coyan, A. D'Amore, Y. Matsumura, D.D. Pedersen, S.K. Luketich, V. Shanov, W.E. Katz, T.E. David, W.R. Wagner, V. Badhwar, *In vivo* functional assessment of a novel degradable metal and elastomeric scaffold-based tissue engineered heart valve, J. Thorac. Cardiovasc. Surg. 157 (2019) 1809–1816, doi:10.1016/j.jtcvs.2018.09.128.
[20] D.L. Morales, C. Herrington, E.A. Bacha, V.O. Morell, Z. Prodán, T. Mroczek, S. Sivalingam, M. Cox, G. Bennink, F.M. Asch, A novel restorative pulmonary valve conduit–Early outcomes of two clinical trials, Front. Cardiovasc. Med. 7 (2021), doi:10.3389/fcvm.2020.583360.
[21] M. Uiterwijk, A.I.P.M. Smits, D. van Geemen, B. van Klarenbosch, S. Dekker, M.J. Cramer, J.W. van Rijswijk, E.B. Lurier, A. Di Luca, M.C.P. Brugmans, T. Mes, A.W. Bosman, E. Aikawa, P.F. Gründeman, C.V.C. Bouten, J. Kluin, *In situ* remodeling overrules bioinspired scaffold architecture of supramolecular elastomeric tissue-engineered heart valves, JACC: Basic to Transl. Sci. 5 (2020) 1187–1206, doi:10.1016/j.jacbts.2020.09.011.
[22] E.S. Fioretta, V. Lintas, A. Mallone, S.E. Motta, L. von Boehmer, P.E. Dijkman, N. Cesarovic, E. Caliskan, H. Rodriguez Cetina Biefer, M. Lipiski, M. Sauer, M. Putti, H.M. Janssen, S.H. Söntjens, A.I.P.M. Smits, C.V.C. Bouten, M.Y. Emmert, S.P. Hoerstrup, Differential leaflet remodeling of bone marrow cell pre-seeded versus nonseeded bioresorbable transcatheter pulmonary valve replacements, JACC: Basic to Transl. Sci. 5 (2020) 15–31, doi:10.1016/j.jacbts.2019.09.008.
[23] R. Duijvelshoff, A. di Luca, E.E. van Haaften, S. Dekker, S.H.M. Söntjens, H.M. Janssen, A.I.P.M. Smits, P.Y.W. Dankers, C.V.C. Bouten, Inconsistency in graft outcome of bilayered bioresorbable supramolecular arterial scaffolds in rats, Tissue Eng. Part A. 27 (13–14) (2021) 894–904, doi:10.1089/ten.tea.2020.0185.
[24] O.J.G.M. Goor, S.I.S. Hendrikse, P.Y.W. Dankers, E.W. Meijer, From supramolecular polymers to multi-component biomaterials, Chem. Soc. Rev. 46 (2017) 6621–6637, doi:10.1039/c7cs00564d.
[25] A. Driessen-Mol, M.Y. Emmert, P.E. Dijkman, L. Frese, B. Sanders, B. Weber, N. Cesarovic, M. Sidler, J. Leenders, R. Jenni, J. Grünenfelder, V. Falk, F.P.T. Baaijens, S.P. Hoerstrup, Transcatheter implantation of homologous "off-the-shelf" tissue-engineered heart valves with self-repair capacity–Long-term functionality and rapid *in vivo* remodeling in sheep, J. Am. Coll. Cardiol. 63 (2014) 1320–1329, doi:10.1016/j.jacc.2013.09.082.
[26] Z. Syedain, J. Reimer, J. Schmidt, M. Lahti, J. Berry, R. Bianco, R.T. Tranquillo, 6 Month aortic valve implantation of an off-the-shelf tissue-engineered valve in sheep, Biomater. 73 (2015) 175–184, doi:10.1016/j.biomaterials.2015.09.016.
[27] T.C. Flanagan, J.S. Sachweh, J. Frese, H. Schnöring, N. Gronloh, S. Koch, R.H. Tolba, T. Schmitz-Rode, S. Jockenhoevel, *In vivo* remodeling and structural characterization of fibrin-based tissue-engineered heart valves in the adult sheep model, Tissue Eng. Part A. 15 (2009) 2965–2976, doi:10.1089/ten.TEA.2009.0018.
[28] S. Dekker, D. van Geemen, A.J. van den Bogaerdt, A. Driessen-Mol, E. Aikawa, A.I.P.M. Smits, Sheep-specific immunohistochemical panel for the evaluation of regenerative and inflammatory processes in tissue-engineered heart valves, Front. Cardiovasc. Med. 5 (2018) 105, doi:10.3389/fcvm.2018.00105.
[29] E. Brauchle, K. Schenke-Layland, Raman spectroscopy in biomedicine - non-invasive *in vitro* analysis of cells and extracellular matrix components in tissues, Biotechnol. J. 8 (2013) 288–297, doi:10.1002/biot.201200163.
[30] J. Marzi, E.M. Brauchle, K. Schenke-Layland, M.W. Rolle, Non-invasive functional molecular phenotyping of human smooth muscle cells utilized in cardiovascular tissue engineering, Acta Biomater. 89 (2019) 193–205, doi:10.1016/j.actbio.2019.03.026.
[31] Z. Movasaghi, S. Rehman, I.U. Rehman, Raman spectroscopy of biological tissues, Appl. Spectrosc. Rev. 42 (2007) 493–541, doi:10.1080/05704920701551530.
[32] S. Hinderer, E. Brauchle, K. Schenke-Layland, Generation and assessment of functional biomaterial scaffolds for applications in cardiovascular tissue engineering and regenerative medicine, Adv. Healthc. Mater. 4 (2015) 2326–2341, doi:10.1002/adhm.201400762.
[33] P. Bankhead, M.B. Loughrey, J.A. Fernández, Y. Dombrowski, D.G. McArt, P.D. Dunne, S. McQuaid, R.T. Gray, L.J. Murray, H.G. Coleman, J.A. James, M. Salto-Tellez, P.W. Hamilton, QuPath–Open source software for digital pathology image analysis, Sci. Rep. 7 (2017) 1–7, doi:10.1038/s41598-017-17204-5.
[34] A. Zbinden, J. Marzi, K. Schlünder, C. Probst, M. Urbanczyk, S. Black, E.M. Brauchle, S.L. Layland, U. Kraushaar, G. Duffy, K. Schenke-Layland, P. Loskill, Non-invasive marker-independent high content analysis of a microphysiological human pancreas-on-a-chip model, Matrix Biol. 85–86 (2020) 205–220, doi:10.1016/j.matbio.2019.06.008.
[35] A. Zbinden, S.L. Layland, M. Urbanczyk, D.A. Carvajal Berrio, J. Marzi, M. Zauner, A. Hammerschmidt, E.M. Brauchle, K. Sudrow, S. Fink, M. Templin, S. Liebscher, G. Klein, A. Deb, G.P. Duffy, G.M. Crooks, J.A. Eble, H.K.A. Mikkola, A. Nsair, M. Seifert, K. Schenke-Layland, Nidogen-1 mitigates ischemia and promotes tissue survival and regeneration, Adv. Sci. 8 (2021) 2002500, doi:10.1002/advs.202002500.
[36] C.L. Jenkins, L.E. Bretscher, I.A. Guzei, R.T. Raines, Effect of 3-hydroxyproline residues on collagen stability, J. Am. Chem. Soc. 125 (2003) 6422–6427, doi:10.1021/ja034015j.
[37] G. Pezzotti, M. Boffelli, D. Miyamori, T. Uemura, Y. Marunaka, W. Zhu, H. Ikegaya, Raman spectroscopy of human skin–Looking for a quantitative algorithm to reliably estimate human age, J. Biomed. Opt. 20 (2015) 065008, doi:10.1117/1.jbo.20.6.065008.
[38] G.J. Mahler, J.T. Butcher, Inflammatory regulation of valvular remodeling–The good(?), the bad, and the ugly, Int. J. Inflam. 2011 (2011) 721419, doi:10.4061/2011/721419.
[39] R. Klopfleisch, F. Jung, The pathology of the foreign body reaction against biomaterials, J. Biomed. Mater. Res. Part A 105 (2017) 927–940, doi:10.1002/jbm.a.35958.
[40] T.B. Wissing, V. Bonito, E.E. van Haaften, M. van Doeselaar, M.M.C.P. Brugmans, H.M. Janssen, C.V.C. Bouten, A.I.P.M. Smits, Macrophage-driven biomaterial degradation depends on scaffold microarchitecture, Front. Bioeng. Biotechnol. 7 (2019) 87, doi:10.3389/fbioe.2019.00087.
[41] H. Talacua, A.I.P.M. Smits, D.E.P. Muylaert, J.W. van Rijswijk, A. Vink, M.C. Verhaar, A. Driessen-Mol, L.A. van Herwerden, C.V.C.V.C. Bouten, J. Kluin, F.P.T. Baaijens, *In situ* tissue engineering of functional small-diameter blood vessels by host circulating cells only, Tissue Eng. Part A 21 (2015) 2583–2594, doi:10.1089/ten.TEA.2015.0066.
[42] N. Hibino, D. Mejias, N. Pietris, E. Dean, T. Yi, C. Best, T. Shinoka, C. Breuer, The innate immune system contributes to tissue-engineered vascular graft performance, FASEB J. 29 (2015) 2431–2438, doi:10.1096/fj.14-268334.
[43] M. Brugmans, A. Serrero, M. Cox, O. Svanidze, F.J. Schoen, Morphology and mechanisms of a novel absorbable polymeric conduit in the pulmonary circulation of sheep, Cardiovasc. Pathol. 38 (2019) 31–38, doi:10.1016/j.carpath.2018.10.008.
[44] K.G. Battiston, R.S. Labow, C.A. Simmons, J.P. Santerre, Immunomodulatory polymeric scaffold enhances extracellular matrix production in cell co-cultures under dynamic mechanical stimulation, Acta Biomater. 24 (2015) 74–86, doi:10.1016/j.actbio.2015.05.038.
[45] K.G. Battiston, B. Ouyang, R.S. Labow, C.A. Simmons, J.P. Santerre, Monocyte/macrophage cytokine activity regulates vascular smooth muscle cell function within a degradable polyurethane scaffold, Acta Biomater. 10 (2014) 1146–1155, doi:10.1016/j.actbio.2013.12.022.
[46] D.T. Ploeger, N.A. Hosper, M. Schipper, J.A. Koerts, S. de Rond, R.A. Bank, Cell plasticity in wound healing–Paracrine factors of M1/M2 polarized macrophages influence the phenotypical state of dermal fibroblasts, Cell Commun. Signal. 11 (2013) 29, doi:10.1186/1478-811X-11-29.
[47] M.C.P. Brugmans, S.H.M. Söntjens, M.a.J. Cox, A. Nandakumar, A.W. Bosman, T. Mes, H.M. Janssen, C.V.C. Bouten, F.P.T. Baaijens, A. Driessen-Mol, Hydrolytic and oxidative degradation of electrospun supramolecular biomaterials–*In vitro* degradation pathways, Acta Biomater. 27 (2015) 21–31, doi:10.1016/j.actbio.2015.08.034.
[48] J.E. McBane, J.P. Santerre, R.S. Labow, The interaction between hydrolytic and oxidative pathways in macrophage-mediated polyurethane degradation, J. Biomed. Mater. Res. A 82 (2007) 984–994, doi:10.1002/jbm.a.31263.
[49] E. Song, N. Ouyang, M. Hörbelt, B. Antus, M. Wang, M.S. Exton, Influence of alternatively and classically activated macrophages on fibrogenic activities of human fibroblasts, Cell. Immunol. 204 (2000) 19–28, doi:10.1006/cimm.2000.1687.
[50] A.K. Capulli, M.Y. Emmert, F.S. Pasqualini, D. Kehl, E. Caliskan, J.U. Lind, S.P. Sheehy, S.J. Park, S. Ahn, B. Weber, J.A. Goss, S.P. Hoerstrup, K.K. Parker, JetValve–Rapid manufacturing of biohybrid scaffolds for biomimetic heart

valve replacement, Biomater. 133 (2017) 229–241, doi:10.1016/j.biomaterials.2017.04.033.
[51] J. Liu, Y. Qin, Y. Wu, Z. Sun, B. Li, H. Jing, C. Zhang, C. Li, X. Leng, Z. Wang, D. Kong, The surrounding tissue contributes to smooth muscle cells' regeneration and vascularization of small diameter vascular grafts, Biomater. Sci. 7 (2019) 914–925, doi:10.1039/c8bm01277f.
[52] T. Pennel, D. Bezuidenhout, J. Koehne, N.H. Davies, P. Zilla, Transmural capillary ingrowth is essential for confluent vascular graft healing, Acta Biomater. 65 (2018) 237–247, doi:10.1016/j.actbio.2017.10.038.
[53] D.E.P. Muylaert, O.G. de Jong, G.G.G. Slaats, F.E. Nieuweboer, J.O. Fledderus, M.-J. Goumans, B.P. Hierck, M.C. Verhaar, Environmental influences on endothelial to mesenchymal transition in developing implanted cardiovascular tissue-engineered grafts, Tissue Eng. Part B Rev. 22 (2016) 58–67, doi:10.1089/ten.teb.2015.0167.
[54] Y. Akatsu, N. Takahashi, Y. Yoshimatsu, S. Kimuro, T. Muramatsu, A. Katsura, N. Maishi, H.I. Suzuki, J. Inazawa, K. Hida, K. Miyazono, T. Watabe, Fibroblast growth factor signals regulate transforming growth factor-β-induced endothelial-to-myofibroblast transition of tumor endothelial cells *via* Elk1, Mol. Oncol. 13 (2019) 1706–1724, doi:10.1002/1878-0261.12504.
[55] S. Piera-Velazquez, S.A. Jimenez, Endothelial to mesenchymal transition–Role in physiology and in the pathogenesis of human diseases, Physiol. Rev. 99 (2019) 1281–1324, doi:10.1152/physrev.00021.2018.
[56] D. van Geemen, A. Driessen-Mol, L.G.M. Grootzwagers, R.S. Soekhradj-Soechit, P.W. Riem Vis, F.P.T. Baaijens, C.V.C. Bouten, Variation in tissue outcome of ovine and human engineered heart valve constructs–Relevance for tissue engineering, Regen. Med. 7 (2012) 59–70, doi:10.2217/rme.11.100.
[57] A.I.P.M. Smits, A. Driessen-Mol, C.V.C. Bouten, F.P.T. Baaijens, A mesofluidics-based test platform for systematic development of scaffolds for *in situ* cardiovascular tissue engineering, Tissue Eng. Part C Methods 18 (2012) 475–485, doi:10.1089/ten.tec.2011.0458.
[58] A.I.P.M. Smits, V. Ballotta, A. Driessen-Mol, C.V.C. Bouten, F.P.T. Baaijens, Shear flow affects selective monocyte recruitment into <scp>MCP</scp>-1-loaded scaffolds, J. Cell. Mol. Med. 18 (2014) 2176–2188, doi:10.1111/jcmm.12330.
[59] C.A. Carruthers, C.M. Alfieri, E.M. Joyce, S.C. Watkins, K.E. Yutzey, M.S. Sacks, Gene expression and collagen fiber micromechanical interactions of the semilunar heart valve interstitial cell, Cell. Mol. Bioeng. 5 (2012) 254–265, doi:10.1007/s12195-012-0230-2.
[60] P. Thayer, K. Balachandran, S. Rathan, C.H. Yap, S. Arjunon, H. Jo, A.P. Yoganathan, The effects of combined cyclic stretch and pressure on the aortic valve interstitial cell phenotype, Ann. Biomed. Eng. 39 (2011) 1654–1667, doi:10.1007/s10439-011-0273-x.
[61] V. Bonito, B.J. de Kort, C.V.C. Bouten, A.I.P.M. Smits, Cyclic strain affects macrophage cytokine secretion and extracellular matrix turnover in electrospun scaffolds, Tissue Eng. Part A 25 (2019) 1310–1325, doi:10.1089/ten.tea.2018.0306.
[62] T.B. Wissing, E.E. Van Haaften, S.E. Koch, B.D. Ippel, N.A. Kurniawan, C.V.C. Bouten, A.I.P.M. Smits, Hemodynamic loads distinctively impact the secretory profile of biomaterial-activated macrophages-implications for *in situ* vascular tissue engineering, Biomater. Sci. 8 (2020), doi:10.1039/c9bm01005j.
[63] E.E. Van Haaften, T.B. Wissing, N.A. Kurniawan, A.I.P.M. Smits, C.V.C. Bouten, Human *in vitro* model mimicking material-driven vascular regeneration reveals how cyclic stretch and shear stress differentially modulate inflammation and matrix deposition, Adv. Biosyst. 4 (2020) 1900249, doi:10.1002/adbi.201900249.
[64] C.A. Best, J.M. Szafron, K.A. Rocco, J. Zbinden, E.W. Dean, M.W. Maxfield, H. Kurobe, S. Tara, P.S. Bagi, B.V. Udelsman, R. Khosravi, T. Yi, T. Shinoka, J.D. Humphrey, C.K. Breuer, Differential outcomes of venous and arterial tissue engineered vascular grafts highlight the importance of coupling long-term implantation studies with computational modeling, Acta Biomater. 94 (2019) 183–194, doi:10.1016/j.actbio.2019.05.063.
[65] R. Khosravi, A.B. Ramachandra, J.M. Szafron, D.E. Schiavazzi, C.K. Breuer, J.D. Humphrey, A computational bio-chemo-mechanical model of *in vivo* tissue-engineered vascular graft development, Integr. Biol. 12 (2020) 47–63, doi:10.1093/intbio/zyaa004.
[66] Y.-L. Wu, J.M. Szafron, K.M. Blum, J.C. Zbinden, R. Khosravi, C.A. Best, J.W. Reinhardt, Q. Zeng, T. Yi, T. Shinoka, J.D. Humphrey, C.K. Breuer, Y. Wang, Electrospun tissue-engineered arterial graft thickness affects long-term composition and mechanics, Tissue Eng. Part A 00 (2020) 1–11, doi:10.1089/ten.tea.2020.0166.
[67] S.E. Motta, E.S. Fioretta, V. Lintas, P.E. Dijkman, M. Hilbe, L. Frese, N. Cesarovic, S. Loerakker, F.P.T. Baaijens, V. Falk, S.P. Hoerstrup, M.Y. Emmert, Geometry influences inflammatory host cell response and remodeling in tissue-engineered heart valves in-vivo, Sci. Rep. 10 (2020) 19882, doi:10.1038/s41598-020-76322-9.
[68] S. Jiang, C. Lyu, P. Zhao, W. Li, W. Kong, C. Huang, G.M. Genin, Y. Du, Cryoprotectant enables structural control of porous scaffolds for exploration of cellular mechano-responsiveness in 3D, Nat. Commun. 10 (1) (2019) 3491, doi:10.1038/s41467-019-11397-1.
[69] E.E. Van Haaften, T.B. Wissing, M.C.M. Rutten, J.A. Bulsink, K. Gashi, M.A.J. van Kelle, A.I.P.M. Smits, C.V.C. Bouten, N.A. Kurniawan, Decoupling the effect of shear stress and stretch on tissue growth and remodeling in a vascular graft, Tissue Eng. Part C Methods 24 (2018) 418–429, doi:10.1089/ten.tec.2018.0104.
[70] Y. Matsuzaki, R. Iwaki, J.W. Reinhardt, Y.-C. Chang, S. Miyamoto, J. Kelly, J. Zbinden, K. Blum, G. Mirhaidari, A. Ulziibayar, T. Shoji, C.K. Breuer, T. Shinoka, The effect of pore diameter on neo-tissue formation in electrospun biodegradable tissue-engineered arterial grafts in a large animal model, Acta Biomater. 115 (2020) 176–184, doi:10.1016/j.actbio.2020.08.011.
[71] D.G. Han, C.B. Ahn, J.H. Lee, Y. Hwang, J.H. Kim, K.Y. Park, J.W. Lee, K.H. Son, Optimization of electrospun poly(caprolactone) fiber diameter for vascular scaffolds to maximize smooth muscle cell infiltration and phenotype modulation, Polymers (Basel) 11 (2019) 643, doi:10.3390/polym11040643.
[72] K. Garg, N. a Pullen, C. a Oskeritzian, J.J. Ryan, G.L. Bowlin, Macrophage functional polarization (M1/M2) in response to varying fiber and pore dimensions of electrospun scaffolds, Biomater. 34 (2013) 4439–4451, doi:10.1016/j.biomaterials.2013.02.065.
[73] J. Fu, M. Wang, I. De Vlaminck, Y. Wang, Thick PCL fibers improving host remodeling of PGS-PCL composite grafts implanted in rat common carotid arteries, Small 16 (2020) 1–15, doi:10.1002/smll.202004133.
[74] K.L. Trout, A. Holian, Factors influencing multinucleated giant cell formation *in vitro*, Immunobiol. 224 (2019) 834–842, doi:10.1016/j.imbio.2019.08.002.
[75] A.K. McNally, J.M. Anderson, Phenotypic expression in human monocyte-derived interleukin-4-induced foreign body giant cells and macrophages *in vitro*–Dependence on material surface properties, J. Biomed. Mater. Res. Part A 103 (2015) 1380–1390, doi:10.1002/jbm.a.35280.
[76] J.W. Reinhardt, J. de, D.R. Rosado, J.C. Barker, Y.-U. Lee, C.A. Best, T. Yi, Q. Zeng, S. Partida-Sanchez, T. Shinoka, C.K. Breuer, Early natural history of neotissue formation in tissue-engineered vascular grafts in a murine model, Regen. Med. 14 (2019) 389–408, doi:10.2217/rme-2018-0133.
[77] N. Laurens, P. Koolwijk, P.M. De Maat, Fibrin structure and wound healing, J. Thromb. Haemost. (2006) 932–939, doi:10.1111/j.1538-7836.2006.01861.x.
[78] E. Aikawa, P. Whittaker, M. Farber, K. Mendelson, R.F. Padera, M. Aikawa, F.J. Schoen, Human semilunar cardiac valve remodeling by activated cells from fetus to adult–Implications for postnatal adaptation, pathology, and tissue engineering, Circulation 113 (2006) 1344–1352, doi:10.1161/CIRCULATIONAHA.105.591768.
[79] E. Rabkin-Aikawa, M. Aikawa, M. Farber, J.R. Kratz, G. Garcia-Cardena, N.T. Kouchoukos, M.B. Mitchell, R.A. Jonas, F.J. Schoen, Clinical pulmonary autograft valves–Pathologic evidence of adaptive remodeling in the aortic site, J. Thorac. Cardiovasc. Surg. 128 (2004) 552–561, doi:10.1016/j.jtcvs.2004.04.016.
[80] K. Schenke-Layland, I. Riemann, F. Opitz, K. König, K.J. Halbhuber, U.A. Stock, Comparative study of cellular and extracellular matrix composition of native and tissue engineered heart valves, Matrix Biol. 23 (2004) 113–125, doi:10.1016/j.matbio.2004.03.005.
[81] A.C. Liu, V.R. Joag, A.I. Gotlieb, The emerging role of valve interstitial cell phenotypes in regulating heart valve pathobiology, Am. J. Pathol. 171 (2007) 1407–1418, doi:10.2353/ajpath.2007.070251.
[82] Z.H. Syedain, M.T. Lahti, S.L. Johnson, P.S. Robinson, G.R. Ruth, R.W. Bianco, R.T. Tranquillo, Implantation of a tissue-engineered heart valve from human fibroblasts exhibiting short term function in the sheep pulmonary artery, Cardiovasc. Eng. Technol. 2 (2011) 101–112, doi:10.1007/s13239-011-0039-5.
[83] M. Votteler, D.A.C. Berrio, A. Horke, L. Sabatier, D.P. Reinhardt, A. Nsair, E. Aikawa, K. Schenke-Layland, Elastogenesis at the onset of human cardiac valve development, Development 140 (2013) 2345–2353, doi:10.1242/dev.093500.
[84] S.E. Motta, E.S. Fioretta, P.E. Dijkman, V. Lintas, L. Behr, S.P. Hoerstrup, M.Y. Emmert, Development of an off-the-shelf tissue-engineered sinus valve for transcatheter pulmonary valve replacement–A proof-of-concept study, J. Cardiovasc. Transl. Res. 11 (2018) 182–191, doi:10.1007/s12265-018-9800-6.
[85] J.L. Ashworth, G. Murphy, M.J. Rock, M.J. Sherratt, S.D. Shapiro, C.A. Shuttleworth, C.M. Kielty, Fibrillin degradation by matrix metalloproteinases–Implications for connective tissue remodeling, Biochem. J. 340 (1999) 171–181, doi:10.1042/0264-6021:3400171.
[86] R. Duijvelshoff, M.S. Cabrera, B. Sanders, S. Dekker, A.I.P.M. Smits, F.P.T. Baaijens, C.V.C. Bouten, Transcatheter-delivered expandable bioresorbable polymeric graft with stenting capacity induces vascular regeneration, JACC: Basic to Transl. Sci. 5 (2020) 1095–1110, doi:10.1016/j.jacbts.2020.09.005.
[87] B.J. De Kort, S.E. Koch, T.B. Wissing, M.M. Krebber, C.V.C. Bouten, A.I.P.M. Smits, Immuno-regenerative biomaterials for in situ cardiovascular tissue engineering - Do patient characteristics warrant precision engineering? Advanced Drug Delivery Reviews 178 (2021) 113960, doi:10.1016/j.addr.2021.113960.
[88] P. Zilla, M. Deutsch, D. Bezuidenhout, N.H. Davies, T. Pennel, Progressive reinvention or destination lost? Half a century of cardiovascular tissue engineering, Front. Cardiovasc. Med. 7 (2020) 159, doi:10.3389/fcvm.2020.00159.
[89] B.L. Zhang, R.W. Bianco, F.J. Schoen, Preclinical assessment of cardiac valve substitutes–Current status and considerations for engineered tissue heart valves, Front. Cardiovasc. Med. 6 (2019) 1–9, doi:10.3389/fcvm.2019.00072.
[90] E.E. van Haaften, R. Duijvelshoff, B.D. Ippel, S.H.M. Söntjens, M.H.C.J. van Houtem, H.M. Janssen, A.I.P.M. Smits, N.A. Kurniawan, P.Y.W. Dankers, C.V.C. Bouten, The degradation and performance of electrospun supramolecular vascular scaffolds examined upon *in vitro* enzymatic exposure, Acta Biomater. 92 (2019) 48–59, doi:10.1016/j.actbio.2019.05.037.